Climate Change in Eastern Victoria

Stage 2 Report:

The effect of climate change on storm surges

A Project Undertaken for the Gippsland Coastal Board

by

K.L. McInnes, I. Macadam, G.D. Hubbert,*
D.J. Abbs and J. Bathols

CSIRO Marine and Atmospheric Research
**Global Environmental Modelling Systems*

June 2005

K.L. McInnes, I. Macadam, G.D. Hubbert, D.J. Abbs, J. Bathols*

CSIRO Marine and Atmospheric Research

****Global Environmental Modelling Systems***

Consultancy report for the Gippsland Coastal Board

Important Disclaimer

This report relates to climate change scenarios based on computer modelling. Models involve simplifications of the real physical processes that are not fully understood. Accordingly, no responsibility will be accepted by CSIRO for the accuracy of projections in this report or actions on reliance of this report.

Address for correspondence

Kathleen McInnes

CSIRO Marine and Atmospheric Research
PMB No 1, Aspendale, Victoria, 3195
Telephone (03) 9239 4660
Fax (03) 9239 4444
E-mail Kathleen.McInnes@csiro.au

CSIRO Marine and Atmospheric Research (http://www.cmar.csiro.au) provides scientific advice and solutions on issues involving the atmospheric environment, the climate system, coastal management, sustainable marine resources and industry Our work is directed toward meeting the needs of government, industry and the community.

For more information about climate change, see
http://www.dar.csiro.au/information/climatechange.html

Table of Contents

Executive Summary 5

1 Introduction 9

2 The Effect of Climate Change on Wind Speed 10

3 Hydrodynamic Models and Data 11

3.1 Tide Data 11

3.2 Hydrodynamic Modelling of Storm Surges 12

3.3 Tidal Constants 13

4 Data Analysis, Model Validation and Methodology 16

4.1 Drivers of Storm Surges 16

4.2 Storm Surges 17

4.3 Methodology and Model Validation 20

5 Storm Tide Modelling Results 24

5.1 Storm Surges 24

5.2 Tide Probabilities 28

5.3 Storm Tides 28

5.4 Mean Sea Level Rise 30

6 Subsidence Potential along the Gippsland Coast 32

7 Conclusions and Recommendations for Further Work 34

Acknowledgments 35

References. 36

Executive Summary

This report presents the results of a study undertaken by CSIRO for the Gippsland Coastal Board to assess the impact of future wind speed changes on storm surges along the eastern Victorian coastline. Hydrodynamical modelling and statistical analysis of extreme sea level events are used to develop spatial patterns of storm surge recurrence intervals under present climate conditions and those projected to occur in 2030 and 2070. While analysis of tide gauge data enables the estimation of storm surge probabilities at the locations of the tide gauges, hydrodynamic modelling can be used as a means to extend the information spatially in a dynamically consistent manner. Extreme value analysis is used to evaluate storm surge return periods over longer intervals than those for which tide gauge data are available.

Projections of future wind speed changes were developed from an analysis of thirteen different climate models. Future changes in wind speed varied considerably in both magnitude and sign across the different models considered, and the corresponding ranges of change were used to form uncertainty estimates in the storm surge projections. Projections of annual mean wind speed changes expressed as a percentage change relative to climatological wind speeds over the 1961-1990 period are 1±2% for 2030 and approximately 3±7% for 2070. Similar mid-range changes are estimated for the annual 95th percentile wind speed, which are approximately 1±3% for 2030 and 3±8% for 2070, indicating that the variations across climate models for the 95th percentile wind speeds were slightly larger than for the mean wind speeds. On a seasonal basis, the mid-range projections of mean and 95th percentile wind speed indicate increases in winds over Bass Strait in all seasons except autumn while the upper range of change was positive in all seasons and the lower range of change indicated declining winds in all seasons. The greatest increases occurred in winter, for which the mean wind changes were 2±3% for 2030 and 5±9% for 2070. The corresponding changes in 95th percentile winds were 2±4% for 2030 and approximately 7±12% for 2070.

Table A1: *Projected annual and winter wind speed changes for the Bass Strait expressed as a percentage relative to climatological wind speeds for the 1961 to 1990 period.*

Season	**Mean Wind Speed**			**95th Percentile Wind Speed**		
	2030			**2030**		
	Low	Mid	High	Low	Mid	High
Annual	-1	1	3	-1	1	4
Winter	-1	2	5	-2	2	6
	2070			**2070**		
	Low	Mid	High	Low	Mid	High
Annual	-5	3	10	-6	3	11
Winter	-4	5	14	-6	7	19

Storm surges along the south coast occur year round suggesting that the most appropriate wind speed scenarios to consider are the annual average changes. However storm surges are more common in the winter months, when more severe cold fronts traverse the southern coastline, and the largest increases projected for wind speed occur in winter. Since this could point to a shift to more frequent storms during winter, a 'worst-case' scenario under which the winter changes were applied was also considered.

Tide gauge data from Stony Point in Western Port Bay and Lakes Entrance were used to identify storm surge events and to validate the hydrodynamic model. Investigation of the meteorological drivers of storm surges indicated that at Lakes Entrance 70% of storm surges of at least 0.4 m were due to cold fronts while 23% were due to Tasman lows and

6% were due to east coast lows (Figure A1a–c). At Stony Point, almost 100% of events were due to cold fronts. This result is supported by hydrodynamic modelling of typical examples of each weather system. Cold fronts elevate sea levels along a larger portion of the eastern Victorian coastline while the effect of Tasman lows was confined to the coastline east of Wilsons Promontory (Figure A1 d-e). East coast lows were found to have the most localised influence (Figure A1f).

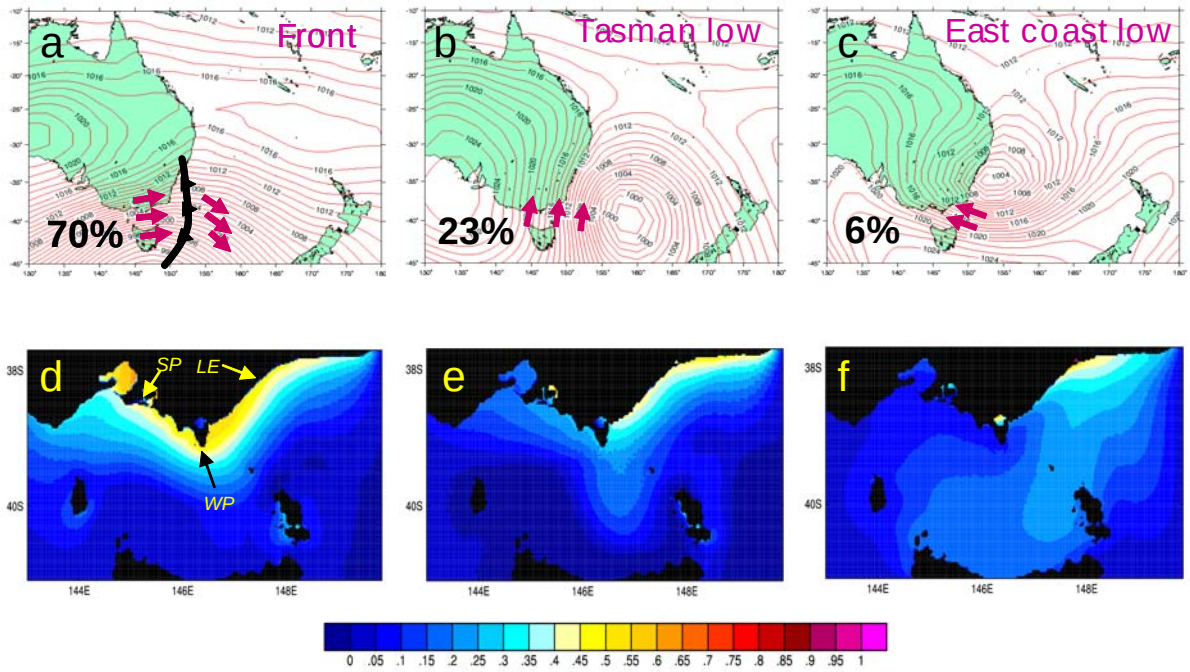

Figure A1: *(a-c) The synoptic weather conditions responsible for storm surges of at least 0.4 m at Lakes Entrance; (d-f)Modelled sea level elevations (m) resulting from examples of each weather type. The locations of Stony Point (SP), Lakes Entrance (LE) and Wilsons Promontory (WP) are indicated on (d).*

A set of 448 storm surge events attaining a level of at least 0.2 m was selected from 23.7 years of tide gauge data. Each event was simulated by forcing the hydrodynamic model with six-hourly wind and pressure fields for the duration of the event. The speeds of the winds were then increased for each event according to the 2070 low, mid and high scenarios of climate change in order to simulate a corresponding set of events occurring under 2070 climate conditions. From these simulations it was established that the storm surge heights increased by approximately 1.9% for each percent wind speed increase. This relationship was used to scale output from the current climate simulations to obtain 2030 low and mid storm surge scenarios (The 2030 high scenario was equivalent to the 2070 mid scenario in terms of wind speed change). Storm surge heights corresponding to each of the wintertime high wind speed scenarios were estimated by scaling the storm surge heights from the appropriate annual high scenario using a regression relationship relating wind speed magnitude to storm surge height so that the mean and 95th percentile wind speed changes could be applied differentially.

A Generalised Pareto Distribution (GPD) was fitted to the set of ranked peak sea levels arising from the 448 events from each set of simulations. The GPD was chosen over the more traditional Generalised Extreme Value distribution because the GPD method makes better use of the available data. The extreme value analysis enabled the calculation of event probabilities and return periods, for which 100 year return levels for various coastal locations are given in Table A2. These values indicate that the highest sea levels during storm surges occur in Western Port Bay (Stony Point) and at Lakes Entrance and the

lowest values occur at Walkerville. Generally, the projected increases in storm surge heights are small owing to the relatively small magnitude storm surges that occur along the Gippsland coast. The high values for annual average wind speed changes for 2030 and 2070 result in approximate increases in storm surge height of 6 and 19% respectively. The 2030 and 2070 high wintertime (JJA) wind speed change scenarios result in approximate increases in the 100 year storm surge level of 6 and 30% respectively.

Table A2: *100 year return levels for storm surge heights at selected locations along the coast under current climate and 2030 and 2070 scenarios.*

Location	Current Climate (m)	2030				2070			
		Low (m)	Mid (m)	High (m)	High JJA (m)	Low (m)	Mid (m)	High (m)	High JJA (m)
Stony Point	0.75 ±0.09	0.73 ±0.09	0.76 ±0.09	0.79 ±0.10	0.80 ±0.10	0.68 ±0.09	0.79 ±0.10	0.88 ±0.10	0.97 ±0.11
Venus Bay	0.60 ±0.08	0.59 ±0.08	0.61 ±0.09	0.65 ±0.10	0.65 ±0.10	0.54 ±0.08	0.65 ±0.10	0.73 ±0.10	0.80 ±0.11
Walkerville	0.56 ±0.10	0.55 ±0.09	0.57 ±0.10	0.59 ±0.09	0.60 ±0.09	0.50 ±0.08	0.59 ±0.09	0.67 ±0.09	0.73 ±0.10
Tidal River	0.64 ±0.09	0.62 ±0.09	0.65 ±0.09	0.64 ±0.08	0.65 ±0.08	0.57 ±0.11	0.64 ±0.08	0.74 ±0.10	0.81 ±0.11
Port Welshpool	0.59 ±0.05	0.58 ±0.05	0.60 ±0.05	0.62 ±0.05	0.62 ±0.05	0.54 ±0.05	0.62 ±0.05	0.69 ±0.06	0.75 ±0.06
Lakes Entrance	0.72 ±0.07	0.70 ±0.06	0.73 ±0.07	0.75 ±0.07	0.76 ±0.07	0.67 ±0.08	0.75 ±0.07	0.83 ±0.07	0.90 ±0.08

The storm surge heights occurring under the low, mid and high scenarios are characterised by fairly uniform changes from the corresponding current climate values. For example, the 2030 low, mid and high scenarios differ from current climate values by approximately -1, 1 and 3 cm respectively across all return periods and locations. For 2070, the low, mid and high scenarios differ from the control climate by -5 to -8, 0 to 4, and 9 to 14 cm respectively. Only the high JJA wind speed changes, which were a function of wind speed, produced an increasing margin of change as the return period increased. The range of increase for the 2030 and 2070 high JJA scenarios are 1 to 5 cm and 15 to 22 cm respectively.

The development of total sea level (storm surge and tide) probabilities required the development of tide height probabilities and the subsequent combination with the surge heights using Monte-Carlo sampling. Prior to developing the tide height probabilities, hydrodynamic modelling was undertaken to develop an improved set of tidal constituent (phase and amplitude) data for Bass Strait. This was necessary because hydrodynamic model simulations of tides in Bass Strait that use tide heights generated by global tide models were found to poorly reproduce the tidal variations at locations across the strait. By running a hydrodynamic model for several months at a time, analysing the tidal constituents from the model output, evaluating errors between modelled and observed tides at the locations of tide gauges, adjusting the values of the constituents along the boundaries and repeating the process iteratively until the errors were minimised, an improved set of tidal constituents was developed for Bass Strait. These were then used to predict tides over a full tidal cycle of 18.6 years and to develop probability distributions for tide heights.

While the highest storm surges along the eastern Victorian coast occur from Lakes Entrance eastwards, the highest tides occur to the west of Wilsons Promontory. The highest storm tides also occur in this region. In combination with the tides, the differences

in sea levels from current climate values are smaller for a given return period than for the storm surge heights alone. Storm tide heights for the 2030 low, mid, high and high JJA scenarios differ from the current climate values by approximately -1, 1, 3 and 5 cm respectively. The 2070 low and mid scenarios exhibit differences of between -6 and -3 cm and between 1 and 5 cm respectively. The differences for the 2070 high and high JJA scenarios are between 7 and 14 cm and 13 and 20 cm respectively. The 2070 high and high JJA scenarios generally exhibit greater margins of increase as return level increases. Port Welshpool exhibits the smallest increases and Stony Point the largest.

Mean sea level rise will have a larger impact on sea level extremes over eastern Victoria than wind speed changes in the future. The 2030 mid and 2070 mid storm tide changes are about 12 to 15 % of the respective mean sea level rise scenarios. The 2030 high and 2070 high wind scenarios produce increases in storm tide height that are about 19% of the respective mean sea level rises. Changes in sea level including both wind speed changes and mean sea level rise are summarised in Table A3 for the 1 in 100 year event.

Table A3: *100 year return levels for the combination of storm tide height and mean sea level rise at selected locations along the coast under current climate and 2030 and 2070 scenarios.*

Location	Current Climate (m)	2030				2070			
		Low (m)	Mid (m)	High (m)	High JJA (m)	Low (m)	Mid (m)	High (m)	High JJA (m)
Stony Point	2.12	2.13	2.24	2.34	2.34	2.14	2.42	2.74	2.81
Venus Bay	1.74	1.76	1.86	1.95	1.96	1.77	2.03	2.36	2.40
Walkerville	1.60	1.61	1.72	1.81	1.81	1.62	1.89	2.20	2.25
Tidal River	1.73	1.74	1.85	1.94	1.95	1.75	2.02	2.33	2.40
Port Welshpool	1.71	1.73	1.83	1.91	1.92	1.74	1.99	2.28	2.35
Lakes Entrance	1.40	1.41	1.51	1.60	1.61	1.41	1.68	2.00	2.06

In addition to possible increases in mean and extreme sea levels at the coast as a result of climate change, flood risk along the coast may be further increased as a result of land subsidence. Although no significant subsidence has been observed, there are concerns that the coastal land surface will start to subside in the future. These are based on borehole measurements that have shown that groundwater levels in the underlying Latrobe Group aquifer have been in decline since 1975. Some estimates suggest that parts of the coast could subside by up to approximately 1 m at some point this century but these results are highly uncertain.

This study has assessed the geophysical hazard posed by storm surges and mean sea level rise along the eastern Victorian coast at a spatial resolution that precludes quantification of the hazard within complex coastal locations such as Lakes Entrance, Corner Inlet and Andersons Inlet. Higher resolution nested modelling would allow the results generated in this study to be extended to these locations.

Other variables are likely to be affected by climate change, the quantification of which would benefit a full coastal vulnerability assessment. These include the occurrence of extreme rainfall events that can accompany the southern Tasman lows and east coast lows that are responsible for about 30% of storm surge events that occur at Lakes Entrance. Rainfall from these systems is likely to increase under climate change and so flood risk within Lakes Entrance due to the combination of extreme sea levels and runoff would be expected to increase also. Wind speed change will impact on the wave heights experienced during extreme storm surge events and these also need to be quantified under climate change scenarios. Finally, changes in the seasonality of extreme wind events were suggested by the analysis conducted in the present study and these needs to be investigated further in relation to the seasonality of extreme sea level events.

1 Introduction

The combined effects of mean sea level rise due to climate change, and changes in the wind patterns associated with severe weather and storms could have significant consequences for Victoria's coastline. The severe winds and falling atmospheric pressures associated with storm events generate higher-than-normal-sea levels at the coast, which are known as storm surges or, in combination with the astronomical tides, as storm tides (see Figure 1). At best, storm tides can increase erosion by increasing the inland penetration of wind waves in the coastal zone and at worst can produce flooding of low-lying coastal terrain. Storm surges can also exacerbate upstream flooding due to severe run-off. Extreme weather events are generally responsible for changes in coastal morphology and damage to coastal infrastructure.

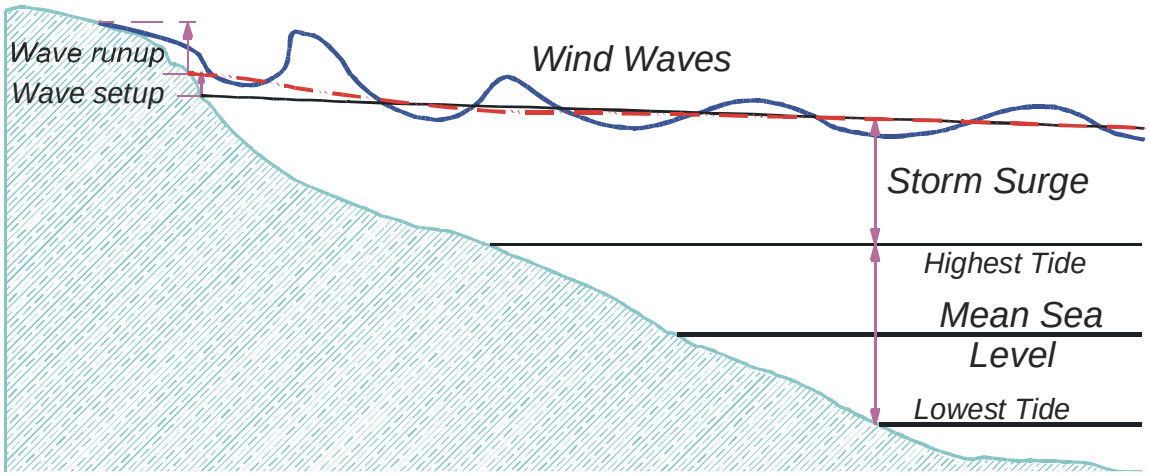

Figure 1: *The contributions to sea level extremes at the coast.*

While estimates of future mean sea level rise are usually factored into coastal impact assessments (see Thieler, 1999 and Sharples, 2004), lack of information on the effect of climate change on extreme events such as storm surges means that they are invariably not considered. Yet there is the potential that the changing frequency and intensity of these temporary sea level events may have more serious implications for the resilience of coasts especially in areas where other pressures such as urbanisation also come to bear.

This study utilizes projections of wind speed changes, developed in the first stage of this project, and hydrodynamical modelling to investigate how storm surges are likely to be affected by a changing climate during the course of this century. Other factors such as mean sea level rise and the possible subsidence of the Gippsland coast are also considered.

The methodology used in this study aims to extend the information that can be obtained from available tide gauges over the region of interest both spatially and temporally. Since the length of the tide gauge record is generally insufficient to determine the recurrence intervals of extreme events for planning purposes, statistical methods for analysing extreme values in data are employed to extrapolate the data to longer return periods. Utilising a hydrodynamic model of the coastal ocean enables the information on storm surge recurrence intervals to be extended to locations other than the tide gauge in a dynamically consistent way. It also enables different climate change scenarios to be simulated.

The remainder of the report is structured as follows: Section 2 summarises the effect of climate change on wind speed over eastern Victoria and section 3 describes the hydrodynamic model and data used in the study. In section 4, the different weather systems that give rise to storm surges and their effect on coastal sea levels over eastern Victoria are presented. A methodology for evaluating storm surge and storm tide probabilities is outlined and the model performance is assessed. Section 5 presents the results of storm surge modelling under various climate change scenarios and combines these results with assessments of tides and mean sea level rise. The possibility of future subsidence along the Gippsland coast is discussed in section 6 and conclusions and recommendations for further work are presented in section 7.

2 The Effect of Climate Change on Wind Speed

The first stage of this project saw the development of climate projections of both mean and 95th percentile near-surface (10 m) wind speeds in the Bass Strait area for the years 2030 and 2070. Following a well established methodology for preparing projections of meteorological variables, described in Whetton et al (in preparation), the climate projections were based upon data from thirteen computer models. These thirteen models were selected from a greater number of internationally recognised climate models on the basis of their superior ability to represent the seasonal features of the climate and patterns of atmospheric circulation of southeastern Australia. Of the thirteen models, five were CSIRO models and three of these were high resolution 'Regional Climate Models', the highest resolution of which was capable of representing atmospheric features on the scale of about 60 km. All of the other ten models were global in their coverage and were capable of representing atmospheric features on the scale of several hundred kilometres. In the development of the projections the thirteen models were assumed to be equally skilled at projecting changes in near-surface wind speeds.

In the first stage of this project the projections were presented as maps of the Bass Strait area showing likely ranges of wind speed changes for 2030 and 2070 (see McInnes et al 2005) The ranges shown incorporated three sources of uncertainty:

- the uncertainty in future emissions of greenhouse gases, as deemed plausible by the Intergovernmental Panel on Climate Change's Special Report on Emissions Scenarios (IPCC, 2000);
- the uncertainty in the sensitivity of the climate system to greenhouse gas emissions, as represented by the thirteen models;
- the spatial variations of change simulated by the different models.

Although the projections were presented as spatial maps of change, the variation of projected wind speed changes across the Bass Strait was small. Hence it has been possible to calculate meaningful areal average low, mid-range and high changes representing the ranges of change for the Bass Strait. These are presented in Table 1.

Table 1 shows that there is considerable uncertainty in the changes in wind speed that can be expected for the Bass Strait. The mid-range value for each season represents an average of the changes suggested by all the models considered. The uncertainty in these projections was estimated from the most extreme model simulations either side of the average value.

For annual average winds, a 1±2% change in mean winds is projected for 2030 and approximately a 3±7% change for 2070. The 95th percentile annual average winds exhibit the same mid-range magnitude of change as the mean winds but the uncertainty is slightly larger with values of approximately 1±3% in 2030 and 3±8% in 2070. On a seasonal basis, the largest mid-range values for mean and 95th percentile winds are seen

in winter, in which the range of change in average winds is 2±3% by 2030 and 5±9% by 2070. The 95th percentile wind speed changes for winter are 2±4% by 2030 and approximately 7±12% by 2070.

It is interesting that the only season that consistently exhibits future decreases in both mean and 95th percentile winds is autumn. For the region under consideration, mid-latitude storms are the major cause of severe wind conditions from late autumn through to spring and this result may point to a shift in the seasonality of such storms under future climate conditions. It is possible that climate change may delay the onset of the storms until the period between winter and early summer. However more detailed investigation of the climate models is required to understand what is driving these changes.

Table 1: *Projected percentage wind speed changes for the Bass Strait (relative to climatological wind speeds for the 1961-1990 period).*

Season	Mean Wind Speed			95th Percentile Wind Speed		
	2030			2030		
	Low	Mid	High	Low	Mid	High
Annual	-1	1	3	-1	1	4
Summer	-1	1	2	-3	0	3
Autumn	-3	-1	1	-6	-2	2
Winter	-1	2	5	-2	2	6
Spring	-2	1	3	-3	0	3
	2070			2070		
	Low	Mid	High	Low	Mid	High
Annual	-5	3	10	-6	3	11
Summer	-3	2	7	-9	1	10
Autumn	-9	-3	3	-19	-6	8
Winter	-4	5	14	-6	7	19
Spring	-6	2	9	-10	-1	8

3 Hydrodynamic Models and Data

3.1 Tide Data

Tide gauge data were required for the purposes of identifying extreme sea level events and for validating model performance. Tide gauge data were obtained from the National Tidal Centre of the Australian Bureau of Meteorology for the tide gauge at Stony Point. This tide gauge has been operating since 1993. Also available from the NTC were sea level residuals calculated by subtracting the predicted tides at the location of the gauge from the measured sea level. The residual signal is a measure of the effect of the weather on the sea levels. McInnes and Hubert (2003) have noted that at locations in Bass Strait tide gauge residuals calculated in this way retain a portion of the tidal signal during severe westerly wind events. These are the events that are responsible for the greatest positive residuals. McInnes and Hubbert hypothesised that the stronger westerly currents interact with the tidal currents leading to a small and temporary phase shifts in the tides.

An alternative method for evaluating tidal residuals, which involves filtering out the tidal signal from the measured sea levels was therefore employed. A Godin moving average filter (Godin, 1972) was applied to the full sea level record from the Stony Point gauge.

The residuals calculated by the two approaches are compared in Figure 1 for May 1994. During this particular month, three successive cold fronts passed through Bass Strait leading to peaks in the residual sea levels on the 17th, 21st and 26th. The filtered residuals are smoother and have lower peak values than the residuals calculated by subtracting the predicted tides. It is these filtered residuals that are used to assess storm tide return periods in the present study.

A tide record has been compiled from several tide gauges operating in Lakes Entrance from January 1974 to December 2001 (Grayson et al, 2004, Tan and Grayson, 2002). Sea level residuals at this location were also calculated by filtering out the astronomical tide from the observed sea levels. Due to periods of missing data, the available data amounted to a 22.5 year record.

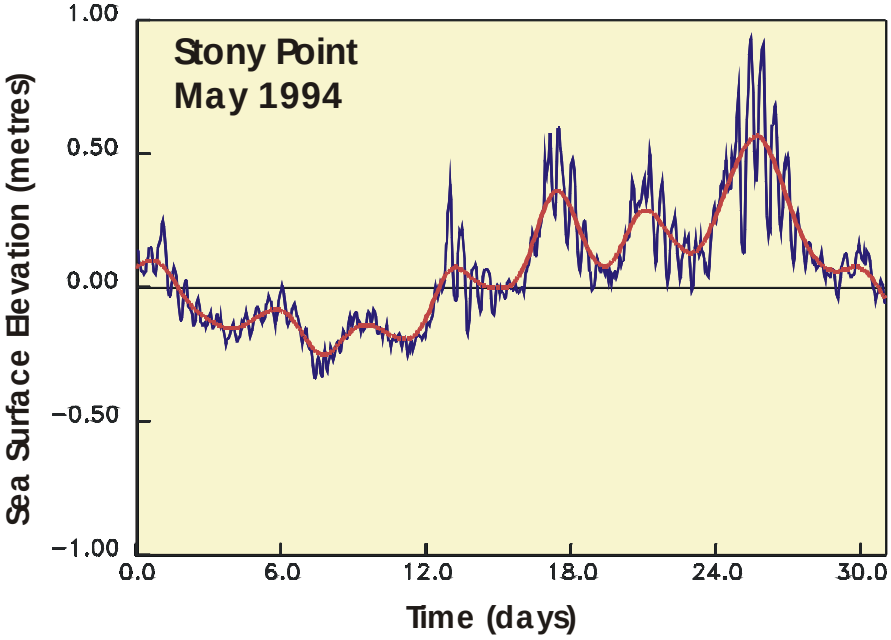

Figure 1: *Sea level residuals calculated by subtracting the predicted tide from the measured sea level (blue curve) with those calculated by filtering the measured sea level signal (red curve).*

3.2 Hydrodynamic Modelling of Storm Surges

The coastal ocean model GCOM2D (Hubbert and McInnes, 1999) solves depth-averaged hydrodynamic equations over a computational grid defined by topographic and bathymetric data over the region of interest to provide currents and sea level heights due to tides and meteorological conditions. In the present study, it has been set up over the region shown in Figure 2 with a grid separation of approximately 1 km. A geographical region that covers Bass Strait has been chosen because of the finding of McInnes and Hubbert (2003) that sea level heights within Bass Strait during westerly wind events can be significantly underestimated if the narrow shelf region in the vicinity of Portland is excluded from the computational domain.

The simulation of storm surges requires that the hydrodynamic model be forced with near-surface winds (typically winds at 10 m above the surface) and surface pressure. These meteorological variables can be derived from either archived analyses of observed weather conditions or atmospheric models. The meteorological conditions for each event are interpolated spatially and temporally to the GCOM2D grid. At the conclusion of each

simulation, the maximum sea level attained at each model grid point is stored as an array of peak sea level values.

The atmospheric data required for the current study were obtained from two sources. For the purposes of exploring the spatial influence of different storm systems on the storm surge, a simple 'parametric' storm model based on Bijl (1997) was used to construct the atmospheric wind and pressure fields associated with the different classes of weather system that cause extreme sea level events. The parametric storm model is a simple tool for generating wind and pressure fields associated with particular weather situations. It is not expected to represent the full field of synoptic scale features with a high degree of accuracy.

In the current study, the main application of GCOM2D is to simulate a population of 'events' that typically range in duration from a day to a week to provide a set of storm surge values that can be analysed to produce event probabilities. For each of the storm surge events identified in the tide gauge records, fields of pressure and winds from gridded reanalyses were used to provide the forcing for GCOM2D. Reanalysis refers to a process whereby a numerical weather prediction model, constrained by available meteorological observations, is used to construct fields of atmospheric data at regular space and time intervals. The reanalysis fields were obtained from the U.S. National Center for Environmental Prediction (NCEP). Surface (10 m) wind fields were available on a 1.875°×1.875° global grid and mean sea level pressure fields were available on a 2.5°×2.5° global grid. The NCEP data is available every six hours from 1958 to the present.

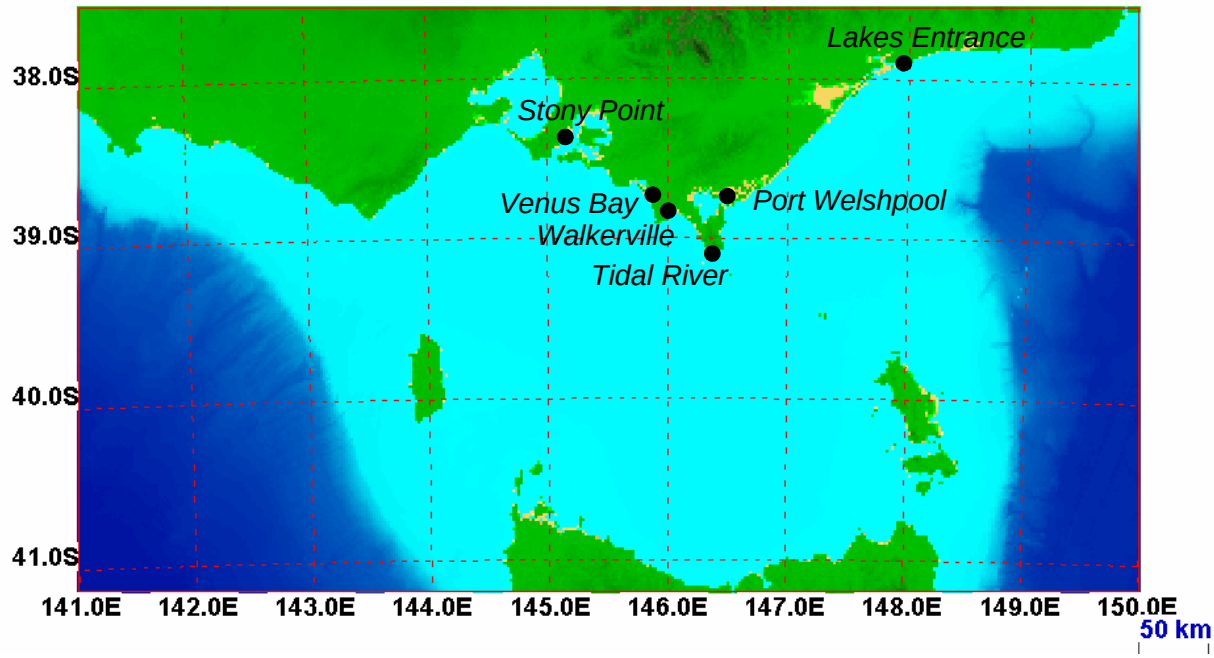

Figure 2: *The horizontal domain of the storm surge model.*

3.3 Tidal Constants

Hydrodynamic models, when used to simulate tides, require knowledge of the tidal heights at their lateral boundaries. The applied tidal forcing is then propagated throughout the computational domain. The source of the tidal components or constituents needed to compute the tide on the boundaries is a global database of tidal constituents available at 30 minute spatial resolution that was developed using a global tide model which models

tidal currents and assimilates satellite measurements of ocean surface heights from the TOPEX/POSEIDON altimeters (Le Provost et al, 1995). These data are accurate to within 0.2-0.3 m in waters deeper than 200 m but are generally inaccurate in shallow coastal waters.

Hydrodynamic models can also be used to develop more accurate tidal constituents in complex coastal regions. This is accomplished by running the model continuously over several tidal cycles and analysing the model output at each grid point to develop a refined set of tidal constituents.

The tides in Bass Strait are complex due to the interaction of the tidal wave with Bass Strait and Tasmania. The westward propagating tidal wave enters Bass Strait at the eastern boundary and also propagates around Tasmania to enter from the west about three hours later. The net effect is that the flood tide enters Bass Strait from both the east and the west and the ebb tide drains out in both directions, albeit separated by a phase difference of up to three hours.

Due to the complex nature of tides in Bass Strait, GCOM2D, when forced with tides predicted using the global tidal constituents, demonstrated poor agreement between modelled and observed tides in this region. As a consequence of this, the three-dimensional counterpart to GCOM2D, GCOM3D, was used to develop improved tidal constituents. GCOM3D (Hubbert, 1993a,b) calculates water currents in both the horizontal and vertical planes. This is important for representing tides accurately because seabed friction affects the vertical gradient of tidal currents and hence the phase and amplitude of tides at the coast.

A model simulation was carried out at 1.5 km horizontal resolution over Bass Strait and Tasmania for several months using tidal heights from the global tidal model as deep water boundary conditions. The time series of tide heights were then subjected to analysis at each model grid point to obtain an improved set of tidal phases and amplitudes. An iterative approach was adopted that involved running the model over several tidal cycles, calculating the root mean square (RMS) errors of phase and amplitude of the modelled constituents at locations where tide gauge data existed and adjusting the boundary conditions until the RMS errors were minimised.

The RMS errors for four of the major tidal constituents; the lunar semidiurnal component, M2, the solar semidiurnal component, S2, the lunisolar diurnal constituent, K1, and the lunar diurnal constituent, O1, calculated using data from 74 tide gauge stations around the coasts of Victoria and Tasmania are summarized in Table 2. In this table the RMS errors based on existing data from a global tide model, the ‘global’ data, and the data derived from the high resolution modelling, the ‘high resolution’ data, are given. The table shows that both the amplitude and phase errors for the M2, S2 and K1 constituents are smaller for the high resolution data than for the global data.

The improved tidal constants were then used to predict more accurate amplitude changes in water level on the lateral boundaries of GCOM2D. An example of the improvement to tidal height is shown in Figure 3 for an eight day simulation of GCOM2D under tide-only forcing. These are compared with the tides produced when the global tidal constituents are used to provide tidal amplitudes on the boundary of the model. The largest improvements with respect to tidal phase can be seen at Stony Point and Burnie. Tidal amplitudes are also improved, particularly at Burnie. At Stony Point, there is still a small underestimation of the tidal amplitude of the higher high tide of the day but improvement in the lower high tide is evident. The Lakes Entrance observed and modelled tides are also shown in Figure 3 to compare the difference in tide heights that are produced on the open coastline by the model with those that were measured inside Lakes Entrance.

These indicate that considerable attenuation of the tidal amplitude and a phase delay occurs between the open coastline and the Lakes. Tan (private communication) estimated an 8:5 ratio between the spring tide heights at the open coastline and at the Lakes and a 9:5 ratio between neap tide heights at the two locations.

Table 2: *Amplitude and phase RMS errors for the global and high resolution data sets.*

	Amplitude (m)		Phase (degrees)	
Constituent	Global	High Resolution	Global	High Resolution
M2	0.07	0.04	25	5
S2	0.02	0.01	27	8
K1	0.04	0.02	9	6
O1	0.01	0.01	6	6

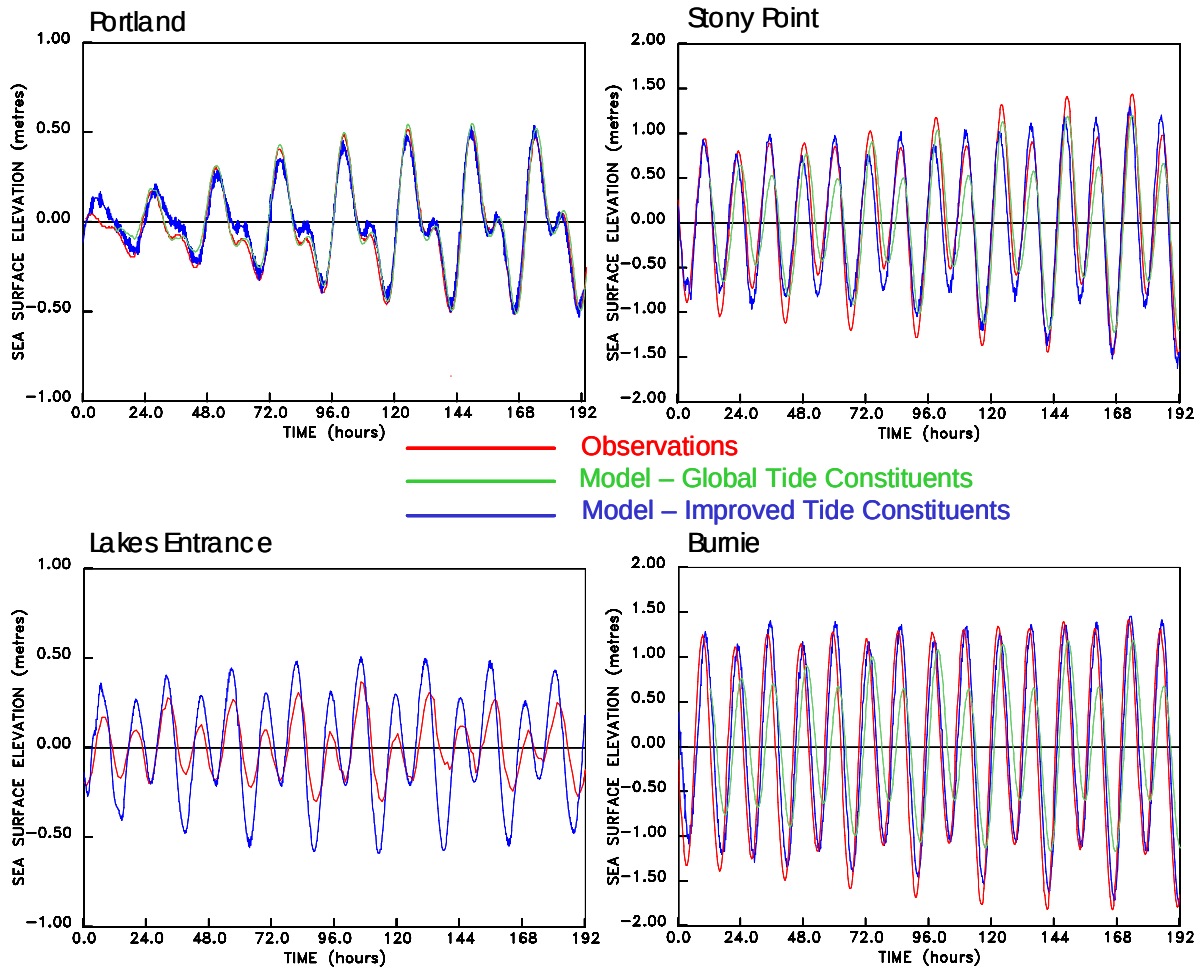

Figure 3: *Comparison of tidal variation over eight days based on tide gauge records and model simulations using global and improved tide constituents at Portland, Stony Point and Burnie. Observed and modelled tides based on improved constituents are also given for Lakes Entrance to illustrate the tidal attenuation that occurs between the open coastline (modelled tides) and the Lakes (observed tides).*

4 Data Analysis, Model Validation and Methodology

4.1 Drivers of Storm Surges

The synoptic weather conditions responsible for elevated sea level events were identified in the first stage of the study. This was achieved by using a synoptic typing technique that identifies similarities in sea level pressure maps using spatial correlation. Lakes Entrance tide gauge data were used to select events for which sea levels were at least 0.4 m above the normal tidal level. Synoptic typing of maps of sea level pressure over southeastern Australia yielded three generic weather patterns. The first, which accounted for 70% of all extreme sea level events at Lakes Entrance, was due to cold fronts at various stages of progression across Bass Strait. This is illustrated in Figure 4a. Winds during these events are generally northwesterly ahead of the front and southwesterly to southerly behind. McInnes and Hubbert (2003) note that these events can elevate sea levels along much of the southeastern coastline of Australia.

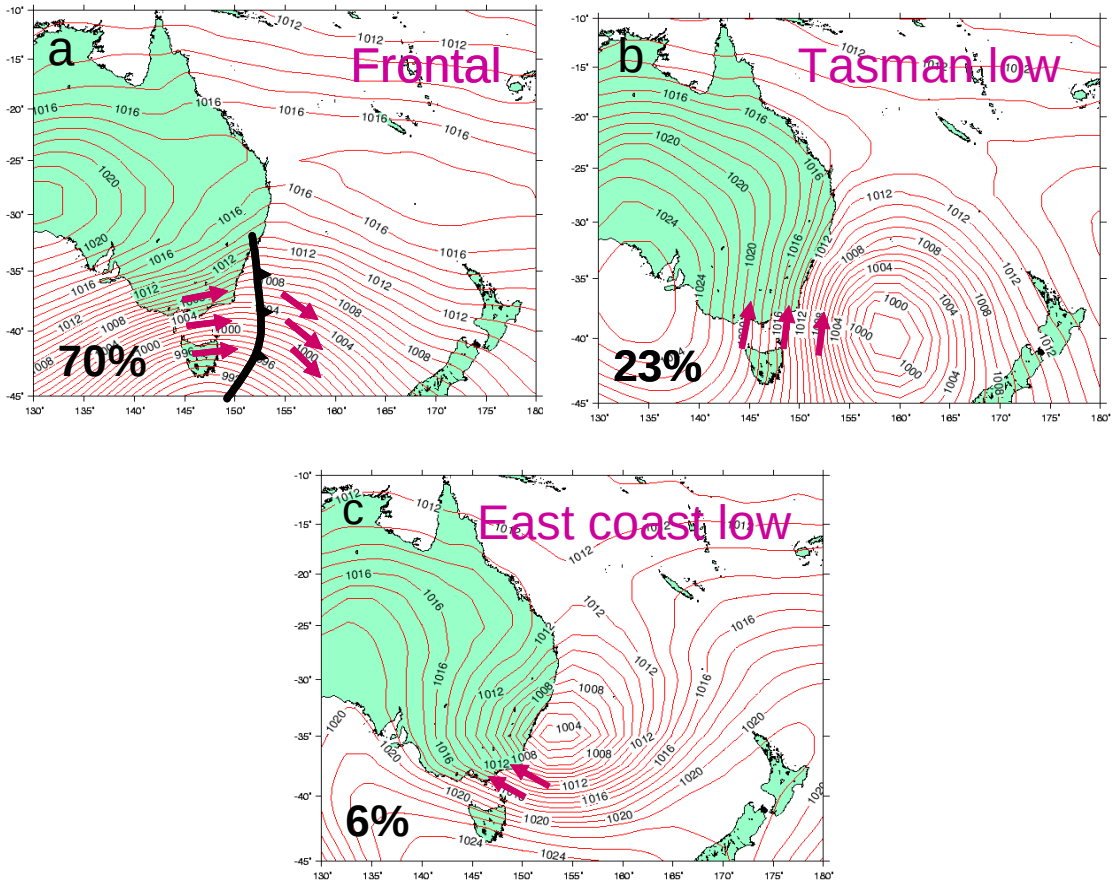

Figure 4: *Synoptic weather conditions leading to elevated sea levels at Lakes Entrance.*

The second most common class of weather pattern responsible for elevated sea levels at Lakes Entrance consisted of a low pressure system in the southern Tasman Sea which produced southerly winds in Bass Strait. It accounted for 23% of cases (Figure 4b). The

third, which accounted for 6% of cases, was a low situated off the east coast with a ridge of high pressure located to the south (Figure 4c). This high-low configuration is known as a blocking pattern and can persist for a number of days since the low is 'cut-off' from the westerlies. The low brings easterly to southeasterly air flow to the east Gippsland coast. These systems can often produce elevated sea levels in combination with high rainfall totals along the southeastern Australian coast (McInnes and Hubbert, 2001).

Synoptic typing was also performed for events of at least 0.4m selected from the Stony Point tide gauge data. At this location, 99% of all events were found to occur in conjunction with the passage of a cold front. A more detailed comparison of the set of events selected from the Stony Point and Lakes Entrance tide gauge data over the 1993 to 2001 period revealed that almost every event of at least 0.4 m selected at Stony Point also occurred at Lakes Entrance. Where events were identified at Stony Point but not Lakes Entrance it was found that data were missing from the Lakes Entrance data set at the time of the event. In a number of cases the Stony Point events preceded the Lakes Entrance events by up to a day.

From these results, two conclusions can be drawn. Firstly, in relation to cold front events, there is strong spatial coherence of extreme sea levels at both Stony Point and Lakes Entrance. In other words, cold fronts elevate sea levels along a substantial length of the Victorian coastline including the region of interest in the present study. Secondly, while additional synoptic weather events were found to be important in generating sea level extremes, their region of influence did not extend as far west as the Stony Point tide gauge. This will be investigated further in section 4.2.

4.2 Storm Surges

To illustrate the typical nature of Bass Strait storm surge events, the characteristic pattern of elevated sea level over this region is modelled using a sequence of wind and pressure patterns generated using a parametric storm model based on the parameters shown in Table 3. Tidal forcing was not applied to the simulations.

Table 3: *Summary of parameters used to construct an example of each of the different synoptic weather types responsible for elevated sea levels at Lakes Entrance. The RMW_{EW} and RMW_{NS} columns give radii of maximum wind speed for low pressure systems in the east-west and north-south directions respectively.*

Synoptic Type	Time (hr)	Central Pressure	Latitude of Centre	Longitude of Centre	RMW_{EW} (km)	RMW_{NS} (km)
Cold Front	0	995	-47.0	143.00	1500	1000
	24	980	-47.0	143.0	1500	1000
	48	975	-45.0	147.0	1000	500
	72	980	-47.0	151.0	1500	1000
	96	995	-47.0	151.0	1500	1000
Tasman Low	0	988	-42.0	150.0	300	300
	12	988	-41.5	150.5	300	300
	24	988	-41.0	151.0	300	300
	36	988	-41.0	151.5	300	300
	48	988	-41.0	152.0	300	300
East Coast Low	0	992	-35.0	152.0	300	300
	12	989	-35.5	151.5	300	300
	24	985	-35.5	151.0	300	300
	36	989	-35.5	151.5	300	300
	48	992	-36.0	152.0	300	300

The cold front example consists of a low to the south of the continent travelling in an eastward direction with the axis of the low greater in the east-west direction. This initially produces northwesterly winds over Bass Strait that turn to a southwesterly direction as the front moves eastwards over a 96 hour interval. The Tasman low consists of a depression situated off the east coast of Tasmania that gradually moves eastwards over a 48 hour interval bringing southeasterly winds to Bass Strait. The low was symmetric with a radius of maximum winds of 300 km. The east coast low example consists of a low situated off the NSW coast, also symmetric with a radius of maximum winds of 300 km, and brings easterly winds to Bass Strait.

The storm surge model was run for each of the examples and the maximum sea level height to occur at each grid point throughout the simulation was recorded. The maxima do not necessarily occur simultaneously. For example, in the frontal event shown in Figure 5, maximum sea levels typically occur earlier in the west and propagate eastwards. The highest open coastline sea levels are found between Western Port Bay and Sale. Inside Port Phillip Bay and Western Port Bay, wind setup produces the highest sea levels on the eastern side of the bays. There is also some elevation of sea levels on the southern and western sides of King and Flinders Islands respectively.

The Tasman low produced the spatial pattern of sea level elevations shown in Figure 5b. Maximum sea levels occur between Lakes Entrance and the border with NSW. The sea level maximum for the east coast low is most localised in its impact with highest sea level elevations situated around Lakes Entrance (see Figure 5c).

The dates and sea level residuals of the top 30 sea level events at Lakes Entrance are summarised in Table 4. The colour-coding indicates the associated synoptic weather pattern. While the most extreme sea level residual recorded was due to a Tasman low, this particular event was also associated with extreme rainfall with the combined runoff into the Lakes estimated to be approximately 550 GL day^{-1} (Grayson et al, 2004) and so some of the elevated sea level within Lakes Entrance was likely due to freshwater run-off. Similarly, the 4th highest event, which was due to an east coast low, was associated with extreme rainfall and the discharge was estimated to be around 480 GL day^{-1}.

Table 4: *Summary of the top 30 events responsible for elevated sea levels at Lakes Entrance. Green refers to Tasman lows, red refers to fronts and blue to east coast lows.*

No	Date (yyyy/mm/dd)			Sea Level (m)	No	Date (yyyy/mm/dd)			Sea Level (m)	No	Date (yyyy/mm/dd)			Sea Level (m)
1	1990	4	26	0.745	11	1974	6	13	0.520	21	1995	6	10	0.485
2	1994	5	26	0.673	12	1978	6	7	0.512	22	1995	7	13	0.483
3*	1994	11	5	0.647	13	1975	5	17	0.511	23	1978	7	4	0.481
4	1998	6	23	0.637	14	1994	1	7	0.498	24	1998	7	28	0.475
5	2000	5	27	0.565	15	1991	8	6	0.496	25	1995	5	25	0.467
6	1974	7	21	0.543	16	1996	9	12	0.493	26	1999	6	13	0.467
7	2001	8	17	0.542	17	1984	7	31	0.487	27	1998	6	28	0.466
8	1988	7	26	0.541	18	1988	10	17	0.487	28	2001	10	31	0.463
9	1996	8	2	0.539	19	1993	9	20	0.487	29	1993	6	13	0.461
10	2000	7	20	0.521	20	1996	11	20	0.487	30	1984	8	12	0.460

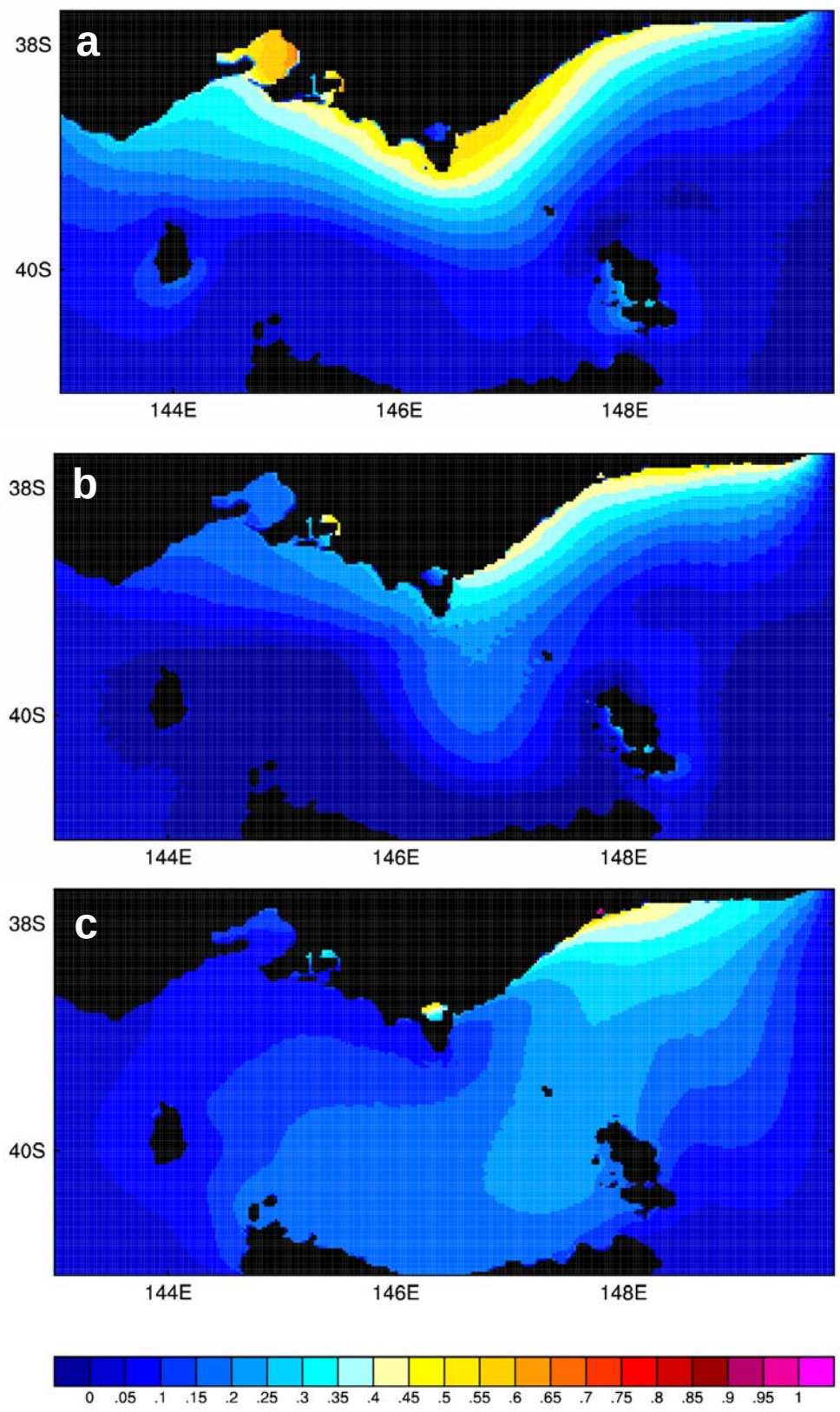

Figure 5: *Spatial patterns of peak sea levels for (a) a cold front, (b) a Tasman low and (c) an east coast low.*

4.3 Methodology and Model Validation

To test the performance of the model, a set of storm surge events was identified in the nine years of Stony Point tide gauge data on the basis that the maximum sea level residual to occur during the event was at least 0.2 m. Stony Point was used in this instance owing to the fact that a more direct comparison of the observed and modelled sea levels could be undertaken at this location. At Lakes Entrance the location of the tide gauge within the Lakes, as opposed to at the open coastal location simulated by the model, means that a direct assessment of model performance is not possible. It is expected that while the sea levels at the open coast and within the Lakes would be comparable for the longer-lived and more extreme events, sea levels within the Lakes during the shorter-lived events may undergo attenuation in the same way as the tides are attenuated by the narrow entrance to the Lakes, as illustrated in Figure 3.

A total of 149 events were selected with durations varying from a day to a week. The six-hourly NCEP wind and pressure data were extracted for the duration of each event, the storm surge model run and the peak sea level at each grid point stored for later analysis. A regression of the observed and modelled sea level events (see Figure 6) shows that the model captures the storm surge response over the entire population of events remarkably well. This is necessary if extreme value analysis is to be used to evaluate return periods for the most extreme events. A comparison of the sea levels for the individual events yielded some discrepancies between modelled and observed events however. This may arise from errors in the wind forcing due to errors in the NCEP reanalyses.

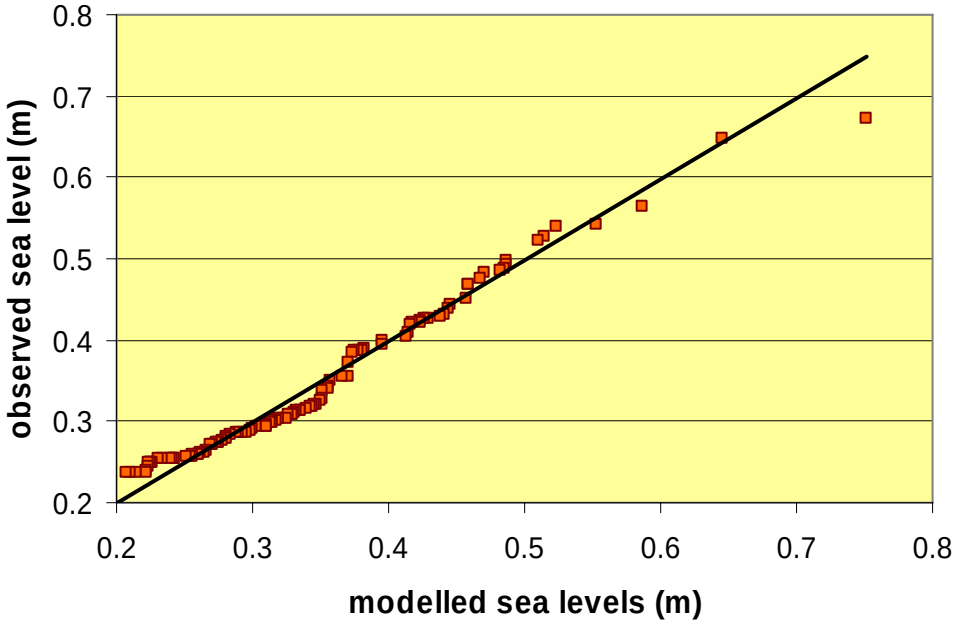

Figure 6: *Regression of observed versus modelled maximum sea level residuals for events where the maximum sea level residual observed at Stony Point exceeded 0.2 m.*

While the events selected from the nine years of Stony Point tide gauge data are useful for the purpose of validating model performance, the Lakes Entrance tide gauge record is longer and experiences storm surges from a broader range of synoptic weather events, indicating that it is the logical record to use for event selection for the storm surge

modelling. However this record contains large gaps meaning that the record which spans 28 years from 1974 to 2001 inclusive, contains only 22.5 years of actual data. Approximately 20% of the data is missing due to changes in custodianship, siting and operation of the three tide gauges that were used to compile the data set.

In this study the number of effective years of data for event selection was increased by filling periods of missing data from 1993 to 2001 with data from the Stony Point gauge. This boosted the effective number of years of data to 23.7. A population of 448 events was selected from this augmented data set. The commencement date of each event selected on the basis of Lakes Entrance gauge data were set at 24 hours before the sea level exceeded 0.2 m at Lakes Entrance and each event ran until the level dropped below 0.2 m again. This was to ensure that the peak of each event was captured further west at Stony Point. Six-hourly wind and pressure data were extracted from the NCEP data set for the duration of each event and interpolated to the storm surge model grid. Each event was simulated and the maximum sea level for each event at each model grid point was stored for subsequent analysis.

The modelled sea level data were then subjected to extreme value analysis to predict the behaviour of rare extreme events on time scales longer than the time period covered by the time series.

Traditional extreme value analysis is based on the Generalised Extreme Value (GEV) distribution (see Coles, 2001), a unification of the Gumbel, Fréchet and Weibull, or, respectively, Type I, II and III, extreme value distributions. A GEV distribution is fitted using only a subset of the data that contains the maximum or minimum values selected from sequences of equal time intervals within the time series. Therefore much of the data contained in the time series is not considered. Furthermore the data that are considered are not necessarily representative of the extreme values of the time series since a time interval may contain more than one extreme value but will only contribute its highest value to the fitting procedure. Conversely another time interval may not contain any extreme values but will still contribute its highest value to the subset.

An alternative to the GEV method of analysing the extreme values of a sample is the extremes-over-threshold or Generalised Pareto Distribution (GPD) method (see Coles, 2001, Holmes and Moriarty, 1999 and Hosking and Wallis, 1987). This involves fitting a GPD to those data in the sample that exceed a certain high threshold, which is chosen to ensure that the GPD is fitted to the large value tail of the sample's probability distribution. The general form of the GPD is

$$F(x) = 1 - (1 - kx/\alpha)^{1/k} \tag{1}$$

where k and α are shape and scale parameters respectively. When the shape parameter is negative (which is generally the case for geophysical distributions), x is restricted to be less than $-1/k$. For the special case of k=0, the GPD reduces to an exponential distribution.

The GPD method of extreme value analysis was applied to time series of sea level residuals from the Stony Point and Lakes Entrance tide gauges. For each time series, sequences of consecutive residuals greater than 0.2 m were identified. The maximum residual in each sequence was then selected and a GPD was fitted to the set of sequence maxima using the maximum likelihood method of parameter estimation (Coles, 2001). This technique ensured that all elevated residual events that fell above the selected threshold were weighted equally in the fitting calculations, irrespective of event duration.

Of the 149 events selected from the nine years of Stony Point observations, the 35 events that fell above a threshold of 0.38 m were found to be sufficiently extreme for a good fit to a GPD to be obtained. Return levels derived from the fitted GPD are illustrated in Figure 7. Of the 413 events selected from the 22.5 years of Lakes Entrance observations, the 146 events that fell above a threshold of 0.32 m were found to be sufficiently extreme for a good fit to a GPD to be obtained. Return levels derived from the fitted GPD are illustrated in Figure 8. Return levels derived from a GEV fitted to annual maximum sea level residuals for Lakes Entrance (not shown) were found to differ from these return levels by less than 0.01m for return periods of greater than 5 years. This suggests that the return levels have a degree of robustness to the method of extreme value analysis used to estimate them.

Return levels derived from GPDs fitted to model data are also shown in Figures 7 and 8. GPDs were fitted to the Stony Point and Lakes Entrance event peaks from the set of 448 modelled events selected from the 23.7 year data set. In each case a good fit was obtained when a GPD was fitted to the greatest 100 event peaks. The corresponding threshold was approximately 0.38 m for Stony Point and 0.44 m for Lakes Entrance. The 0.44 m threshold was applied to a smaller set of Lakes Entrance event peaks from a set of modelled events selected using just the 22.5 years of Lakes Entrance observations and a GPD was fitted. Return levels derived from this GPD (not shown) were found to differ from the return levels estimated from the 448 event data set by less than 0.01m. This suggests that the return levels are robust to the use of data from the Stony Point tide gauge to fill periods of missing data in the Lakes Entrance record. However the resulting increase in the number of events reduced the uncertainties associated with the return periods.

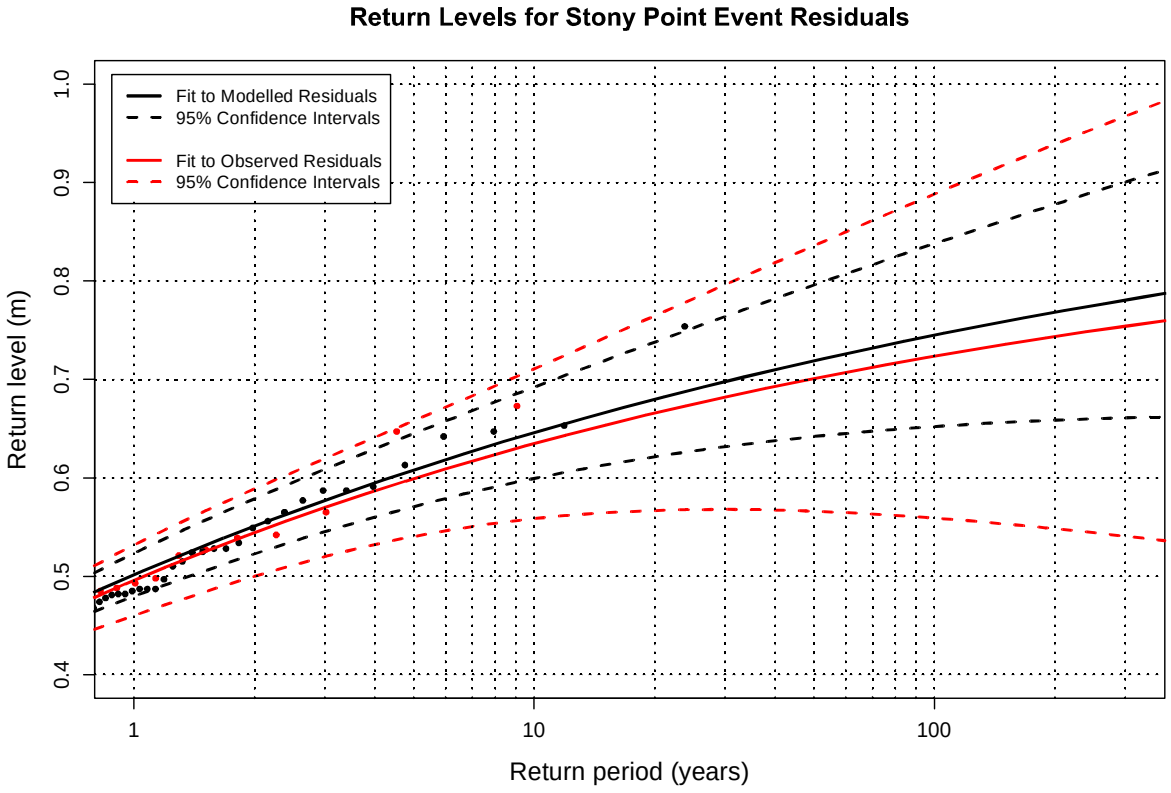

Figure 7: *Return levels for elevated sea level residuals at Stony Point based on a GPD analysis of nine years of observed and 23.7 years of modelled events.*

For Stony Point the modelled event peaks yield a slightly larger sea level residual for a given return period than the nine years of observations. Although close agreement exists between the modelled and observed return period curves, the relatively small amount of observational data compared with the modelled data leads to broader 95% confidence limits associated with the curve of best fit. It is worth noting that return levels estimated from the 149 modelled sea levels shown in Figure 6 were found to be almost identical to those estimated from the observed Stony Point sea levels (not shown).

Figure 8 presents the modelled and observed residuals for Lakes Entrance and indicates that the observations from inside Lakes Entrance behave quite differently from the modelled sea levels on the open coast. In particular, the return period curve based on the observations is much steeper with lower residual values at return periods less than 100 years and higher values at return levels longer than 100 years. There are at least two reasons for the differences. Firstly, the narrow entrance to the Lakes is likely to differentially attenuate the sea levels on the open coast such that the shorter-lived smaller sea level events are likely to suffer more attenuation than the longer-lived more extreme events. This may explain the higher magnitudes of modelled sea levels at return periods shorter than 100 years. The second reason is that the observed sea levels within the Lakes may contain a significant freshwater component during events for which severe rainfall occurs. This is the case for the two most extreme observed events which were major flood events that occurred on 22 April 1990 and 24 June 1998 (Grayson et al, 2004).

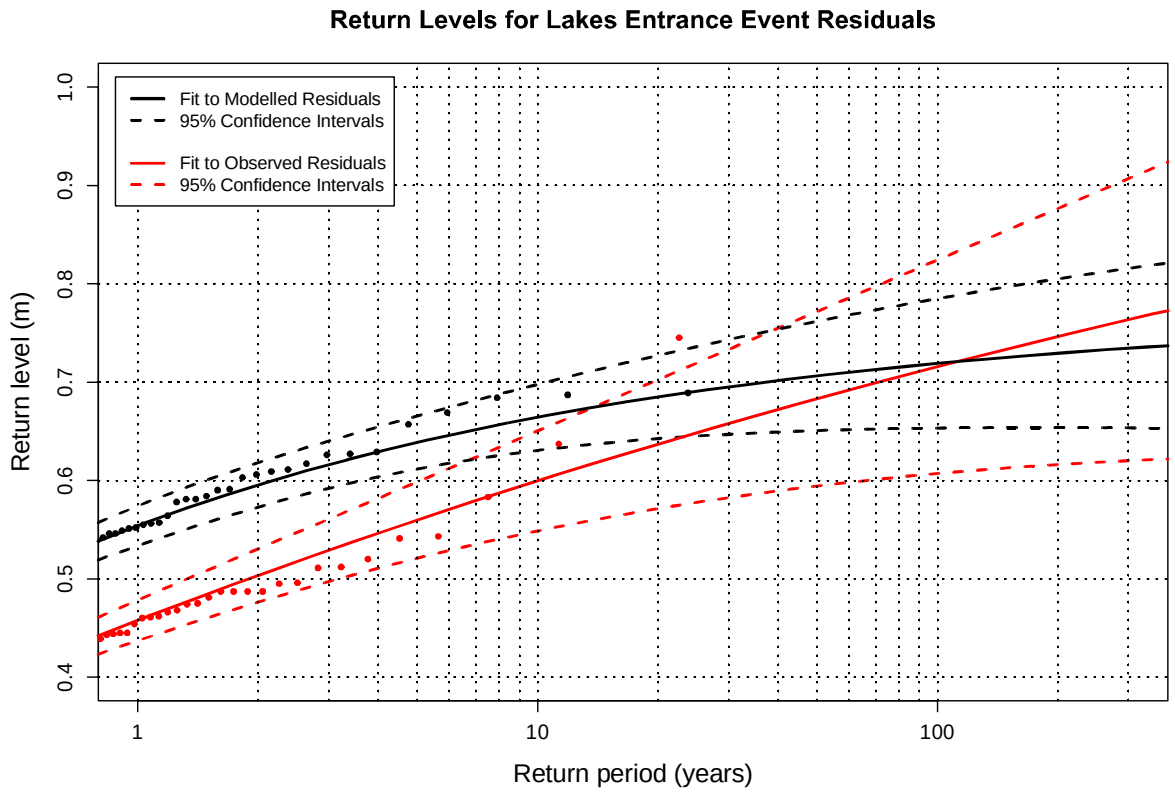

Figure 8: *Return levels for elevated sea level residuals at Lakes Entrance based on a GPD analysis of 22.5 years of observed and 23.7 years of modelled events.*

5 Storm Tide Modelling Results

5.1 Storm Surges

Section 2 revealed that the annual averaged mean and 95th percentile wind speed changes for Bass Strait were of a similar magnitude (see Table 1). In terms of the wind speed distribution, this result is consistent with a change in the mean wind speed with no change occurring in the shape of the distribution. The changes in annual averaged mean wind speed for 2070 were therefore applied to the winds driving each of the 448 selected storm surge events irrespective of the severity of these winds.

The choice of annual wind speed change scenario was made on the grounds that the events selected for modelling occur year round. However, the largest wind speed changes are seen in winter with relatively greater increases occurring for the 95th percentile winds compared to the mean speed changes. It can be argued that the larger winter changes may reflect a change in seasonality of extreme events that cause storm surges. To consider this 'worst case' possibility, an additional scenario that utilised the winter time high scenario mean and extreme wind changes was also considered.

Each of the 448 storm surge events were modelled under current climate conditions and the 2070 annual low, mid and high scenarios. A GPD was fitted to the data from each run at several selected coastal locations. The best fit to the data for a specific scenario and location was usually found when approximately the 100 most extreme data were fitted and so the 100 most extreme data were fitted for all selected scenarios and locations. From the GPD fit, return periods and probabilities of exceedence for peak sea level residuals were calculated. Comparing the average change in storm surge height for each of the 2070 low, mid and high scenarios with the reference climate simulations indicated that, on average, changes in storm surge height were consistently found to be about 1.9 times the wind speed change. In other words, a 10% increase in wind speed led to approximately a 19% increase in storm surge height. This suggested that the 2030 low and mid range scenarios for storm surge height could be calculated by simply scaling the current climate results by the appropriate amount since the departures in wind speed from current climate were only slight. Note that the 2030 high scenario is equivalent to the 2070 mid range scenario.

The winter (JJA) high scenarios for 2030 and 2070 were also developed by scaling the respective annual high values. However, since the winter 95th percentile winds were projected to increase by a greater amount than the mean winds, a method for applying the wind speed changes differentially according to the severity of the storm surge was required. The mean and 95th percentile winds over Bass Strait corresponded to values of 7.2 and 18.4 ms^{-1} respectively. A regression relationship was developed between the maximum six-hourly wind speed and peak storm surge height using the maximum wind speed to occur in the NCEP wind analyses over Bass Strait during each storm surge event. Using the 1:1.9% ratio between wind speed change and storm surge change, multipliers were developed to differentially increase the storm surge heights assuming a linear relationship for wind speed change between the 95^{th} percentile and the mean wind values of change. Examples of the return period curves developed for Venus Bay and Lakes Entrance under the various 2070 scenarios are shown in Figures 9 and 10 respectively and storm surge heights for several return levels are presented in Table 5 for various locations along the coast. The 95% confidence intervals presented in the figures and table are related to the uncertainties in the estimates of the shape and scale parameters of the best fitting GPD.

The return period curves for Venus Bay (Figure 9) are slightly steeper than those for Lakes Entrance (Figure 10). This is due to the shape parameters of the GPDs fitted to the

Venus Bay data taking smaller negative values than the shape parameters of the GPDs fitted to the Lakes Entrance data. The results presented in Table 5 for the low, mid and high scenarios are characterised by fairly uniform changes from respective current climate values across all return periods and locations considered. For example, the 2030 low, mid and high scenarios differ from current climate values by approximately -1, 1 and 3 cm respectively across all return periods and locations. For 2070, the low, mid and high scenarios differ from the control climate by -5 to -8, 0 to 4, and 9 to 14 cm respectively. Only the high JJA wind speed changes, which were a function of wind speed, produced an increasing margin of change as the return period increased. The range of increase for the 2030 and 2070 high JJA scenarios are 1 to 5 cm and 15 to 22 cm respectively.

To develop spatial patterns of storm surge return periods, GPDs ideally should be fitted to the modelled data at each model gridpoint. Although work is progressing to develop this capability, the level of subjectivity in fitting a GPD using conventional methods precluded this in the present study. Instead, return levels for each gridpoint were calculated using return levels estimated from GPDs fitted to the data for the coastal locations shown in Figure 2. A particular return level for an individual gridpoint, z_{ij}, was obtained by multiplying the corresponding return level for the nearest coastal location, z_{loc}, by the ratio of the maximum modelled surge height at the gridpoint, z_{ij}^{max}, to that at the location, z_{loc}^{max}:

$$z_{ij} = z_{loc} \frac{z_{ij}^{\max}}{z_{loc}^{\max}} \qquad (2)$$

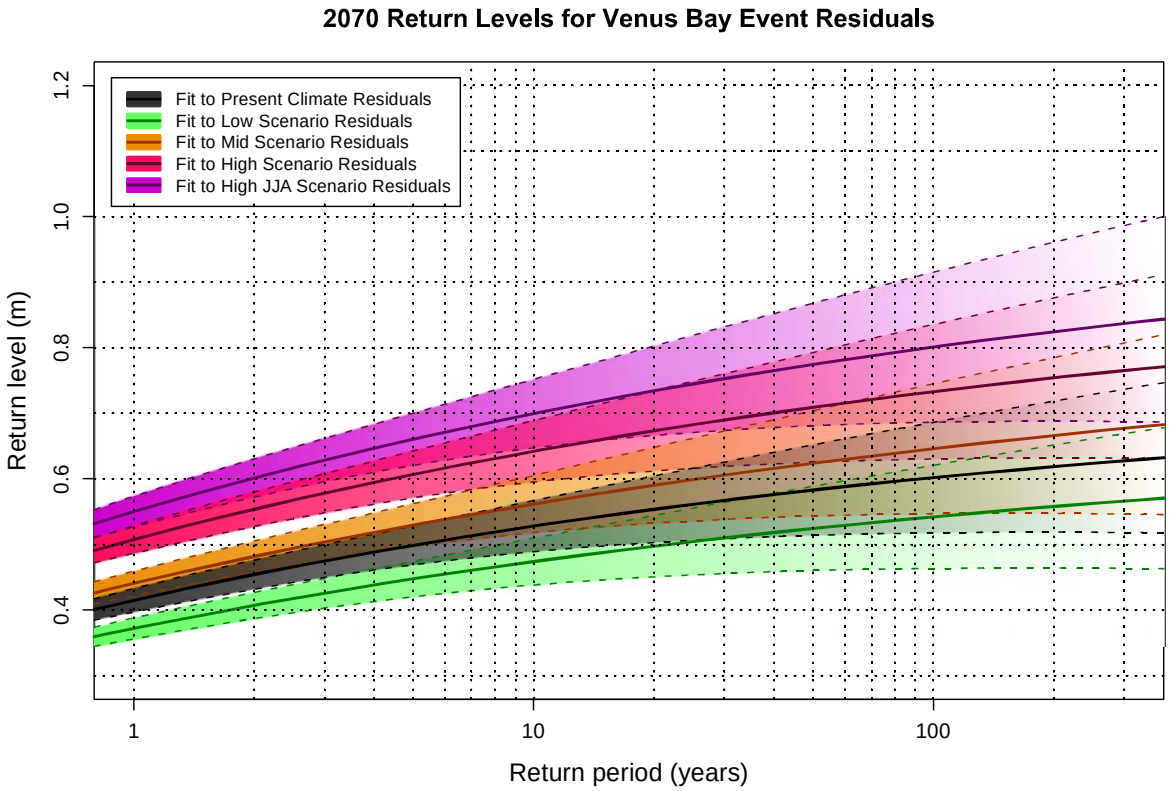

Figure 9: *Return levels developed from the Venus Bay event residuals under current climate conditions, 2070 low, mid and high annual wind change scenarios and the 2070 high winter wind change scenario. The shading around each curve indicates the 95% confidence intervals.*

Figure 11 indicates that the highest 1 in 100 year storm surges occur to the east of Lakes Entrance and exceed 0.7 m. To the west of Wilsons Promontory and along Venus Bay, maximum storm surge heights are between 0.55 and 0.60 m while Walkerville and the eastern side of Wilsons Promontory, which are relatively sheltered from the prevailing winds, experience slightly lower storm surges of between 0.50 and 0.55 m. The highest storm surge heights in Corner Inlet, which exceed 0.55 m, occur in the north.

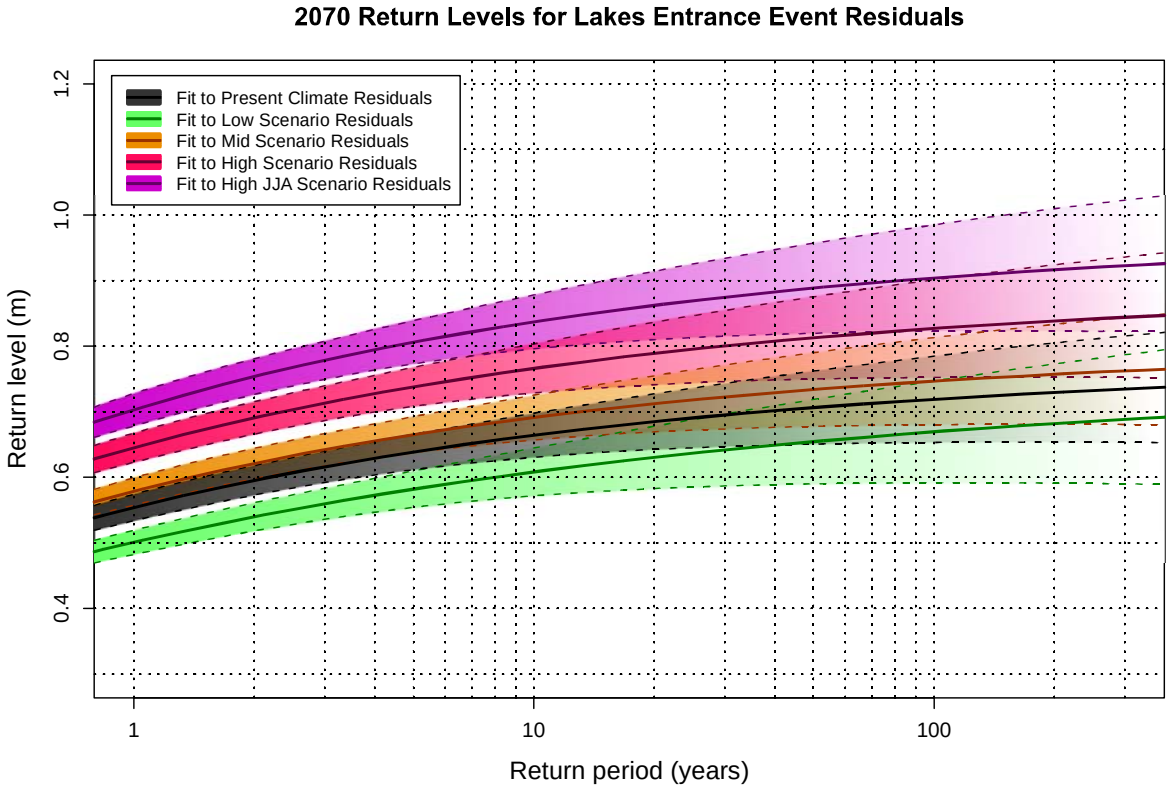

Figure 10: *Return levels developed from the Lakes Entrance event residuals under current climate conditions, 2070 low, mid and high annual wind change scenarios and the 2070 high winter wind change scenario. The shading around each curve indicates the 95% confidence intervals.*

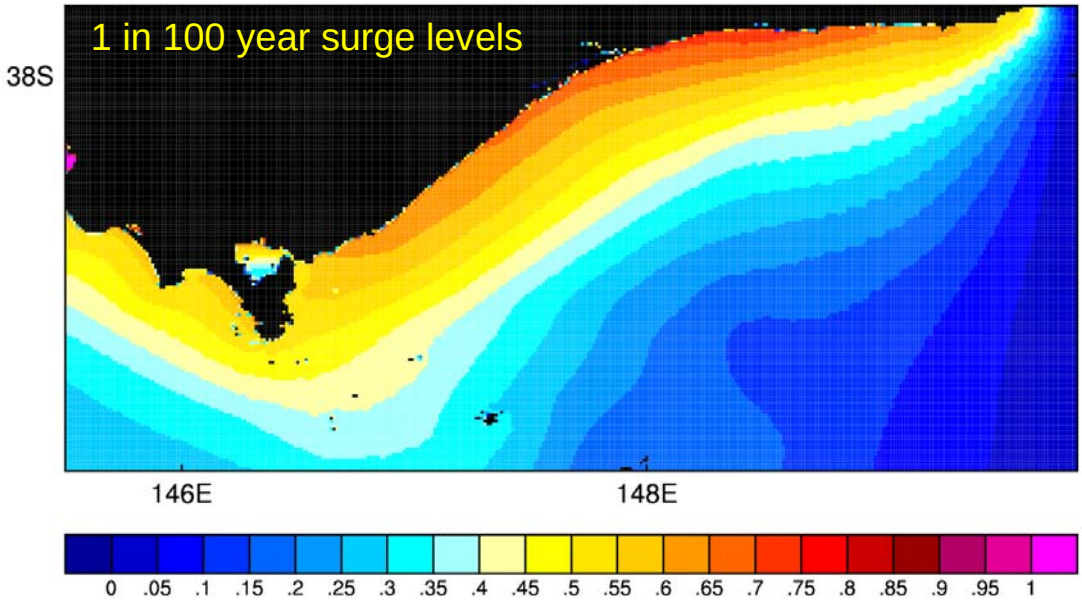

Figure 11: *The spatial pattern of the 1 in 100 year storm surge heights (m) under current climate conditions.*

Table 5: *Storm surge height return levels for selected locations along the coast under current climate and 2030 and 2070 scenarios with 95% confidence intervals.*

Location	Return Period (yr)	Current Climate (m)	2030				2070			
			Low (m)	Mid (m)	High (m)	High JJA (m)	Low (m)	Mid (m)	High (m)	High JJA (m)
Stony Point	10	0.65 ±0.05	0.63 ±0.05	0.66 ±0.05	0.68 ±0.05	0.69 ±0.05	0.58 ±0.04	0.68 ±0.05	0.77 ±0.05	0.85 ±0.06
	20	0.68 ±0.06	0.67 ±0.06	0.69 ±0.06	0.72 ±0.06	0.73 ±0.06	0.62 ±0.05	0.72 ±0.06	0.81 ±0.06	0.89 ±0.07
	50	0.72 ±0.08	0.70 ±0.08	0.73 ±0.08	0.76 ±0.08	0.77 ±0.08	0.65 ±0.07	0.76 ±0.08	0.86 ±0.08	0.94 ±0.09
	100	0.75 ±0.09	0.73 ±0.09	0.76 ±0.09	0.79 ±0.10	0.80 ±0.10	0.68 ±0.09	0.79 ±0.10	0.88 ±0.10	0.97 ±0.11
Venus Bay	10	0.53 ±0.04	0.52 ±0.04	0.54 ±0.04	0.56 ±0.04	0.57 ±0.04	0.47 ±0.04	0.56 ±0.04	0.64 ±0.05	0.70 ±0.05
	20	0.55 ±0.05	0.54 ±0.05	0.56 ±0.05	0.59 ±0.06	0.60 ±0.06	0.50 ±0.05	0.59 ±0.06	0.67 ±0.06	0.73 ±0.07
	50	0.58 ±0.07	0.57 ±0.07	0.59 ±0.07	0.62 ±0.08	0.63 ±0.08	0.52 ±0.06	0.62 ±0.08	0.71 ±0.08	0.77 ±0.09
	100	0.60 ±0.08	0.59 ±0.08	0.61 ±0.09	0.65 ±0.10	0.65 ±0.10	0.54 ±0.08	0.65 ±0.10	0.73 ±0.10	0.80 ±0.11
Walkerville	10	0.48 ±0.04	0.47 ±0.04	0.49 ±0.04	0.51 ±0.04	0.52 ±0.04	0.43 ±0.03	0.51 ±0.04	0.59 ±0.04	0.64 ±0.05
	20	0.51 ±0.05	0.50 ±0.05	0.52 ±0.06	0.54 ±0.05	0.55 ±0.05	0.45 ±0.04	0.54 ±0.05	0.62 ±0.05	0.67 ±0.06
	50	0.54 ±0.08	0.53 ±0.07	0.55 ±0.08	0.57 ±0.07	0.58 ±0.07	0.48 ±0.06	0.57 ±0.07	0.65 ±0.07	0.71 ±0.08
	100	0.56 ±0.10	0.55 ±0.09	0.57 ±0.10	0.59 ±0.09	0.60 ±0.09	0.50 ±0.08	0.59 ±0.09	0.67 ±0.09	0.73 ±0.10
Tidal River	10	0.56 ±0.04	0.55 ±0.04	0.57 ±0.04	0.57 ±0.04	0.58 ±0.04	0.48 ±0.04	0.57 ±0.04	0.66 ±0.05	0.71 ±0.05
	20	0.59 ±0.05	0.57 ±0.05	0.60 ±0.06	0.60 ±0.05	0.60 ±0.05	0.51 ±0.06	0.60 ±0.05	0.68 ±0.06	0.75 ±0.07
	50	0.62 ±0.07	0.60 ±0.07	0.63 ±0.08	0.62 ±0.07	0.63 ±0.07	0.54 ±0.09	0.62 ±0.07	0.72 ±0.08	0.78 ±0.09
	100	0.64 ±0.09	0.62 ±0.09	0.65 ±0.09	0.64 ±0.08	0.65 ±0.08	0.57 ±0.11	0.64 ±0.08	0.74 ±0.10	0.81 ±0.11
Port Welshpool	10	0.54 ±0.03	0.53 ±0.03	0.55 ±0.03	0.57 ±0.03	0.57 ±0.03	0.49 ±0.03	0.57 ±0.03	0.63 ±0.03	0.69 ±0.03
	20	0.56 ±0.03	0.54 ±0.03	0.57 ±0.04	0.59 ±0.03	0.59 ±0.04	0.51 ±0.03	0.59 ±0.03	0.65 ±0.04	0.71 ±0.04
	50	0.58 ±0.04	0.56 ±0.04	0.59 ±0.05	0.61 ±0.04	0.61 ±0.05	0.53 ±0.04	0.61 ±0.04	0.68 ±0.05	0.74 ±0.05
	100	0.59 ±0.05	0.58 ±0.05	0.60 ±0.05	0.62 ±0.05	0.62 ±0.05	0.54 ±0.05	0.62 ±0.05	0.69 ±0.06	0.75 ±0.06
Lakes Entrance	10	0.66 ±0.03	0.65 ±0.03	0.68 ±0.03	0.69 ±0.03	0.70 ±0.03	0.61 ±0.04	0.69 ±0.03	0.77 ±0.04	0.84 ±0.04
	20	0.68 ±0.04	0.67 ±0.04	0.70 ±0.04	0.71 ±0.04	0.72 ±0.04	0.63 ±0.05	0.71 ±0.04	0.79 ±0.05	0.86 ±0.05
	50	0.71 ±0.06	0.69 ±0.05	0.72 ±0.06	0.73 ±0.06	0.74 ±0.06	0.65 ±0.06	0.73 ±0.06	0.81 ±0.06	0.89 ±0.07
	100	0.72 ±0.07	0.70 ±0.06	0.73 ±0.07	0.75 ±0.07	0.76 ±0.07	0.67 ±0.08	0.75 ±0.07	0.83 ±0.07	0.90 ±0.08

5.2 Tide Probabilities

The peak sea levels to occur during a storm surge event depend upon the tides at the time of the surge. To combine the peak storm surge heights with tides, tidal height frequency distributions were developed at each model grid point by running a tide prediction model over a full tidal cycle (18.6 years). Since tides are semidiurnal in Bass Strait and the duration of storm surges in Bass Strait is typically several days for the larger events, tide frequency distributions were developed for the high tide values. When combining the peak storm surge with the tides, it was assumed that the storm surge stayed close to its peak for at least twelve hours thereby coinciding with a high tide. The spatial pattern of the mean higher high water levels (the average of the daily higher high tide) is shown in Figure 12 and indicates that the highest sea levels in Bass Strait occur along Tasmania's northern coast.

Along the Victorian coast the highest tides occur between Western Port Bay and Wilsons Promontory while the lowest tides occur along Ninety Mile Beach. The highest sea levels during high tides occur in a region that traverses central Bass Strait. This pattern of high tides occurs because the westward propagating tidal wave enters Bass Strait not only at the eastern boundary but also travels around Tasmania to enter from the west about three hours later. The net effect is that the highest tides are produced in the centre of Bass Strait where the two tidal currents meet.

5.3 Storm Tides

The storm surges were combined with the tides using a Monte-Carlo approach whereby 8000 storm surge and tide heights were randomly sampled from their respective probability distributions and summed. This approach was adopted because it would have been prohibitively computationally expensive to fully explore the possible surge and tide combinations using the hydrodynamical model. Storm tide heights estimated by the Monte-Carlo method will be slightly greater than those estimated by the hydrodynamical modelling method. This is because a storm of a particular magnitude will produce a slightly lower storm surge if it coincides with high tide heights than if it coincides with lower tide heights. The storm tide heights obtained via the Monte-Carlo method were ranked, a rank of 1 being assigned to the greatest height and 8000 to the least, and the return periods in years were calculated using

$$R = \frac{1}{r}\frac{N}{\lambda} \tag{3}$$

where r is the rank of the storm tide height, N is the total number of sampled events and λ is the number of events that occur each year (N/λ is the number of years that are represented by the sample of events). The spatial pattern of the 1 in 100 year storm tide is shown in Figure 13. The highest total sea levels occur to the west of Wilsons Promontory where the tidal range and storm surge heights both tend to be large.

Storm tide height return levels for selected locations are presented in Table 6. Storm tide heights for the 2030 low, mid, high and high JJA scenarios differ from the current climate values by approximately -1, 1, 3 and 5 cm respectively. The 2070 low and mid scenarios exhibit differences of between -6 and -3 cm and between 1 and 5 cm respectively. The differences for the 2070 high and high JJA scenarios are between 7 and 14 cm and 13 and 20 cm respectively. The 2070 high and high JJA scenarios generally exhibit greater margins of increase as return level increases. Port Welshpool exhibits the smallest increases and Stony Point the largest.

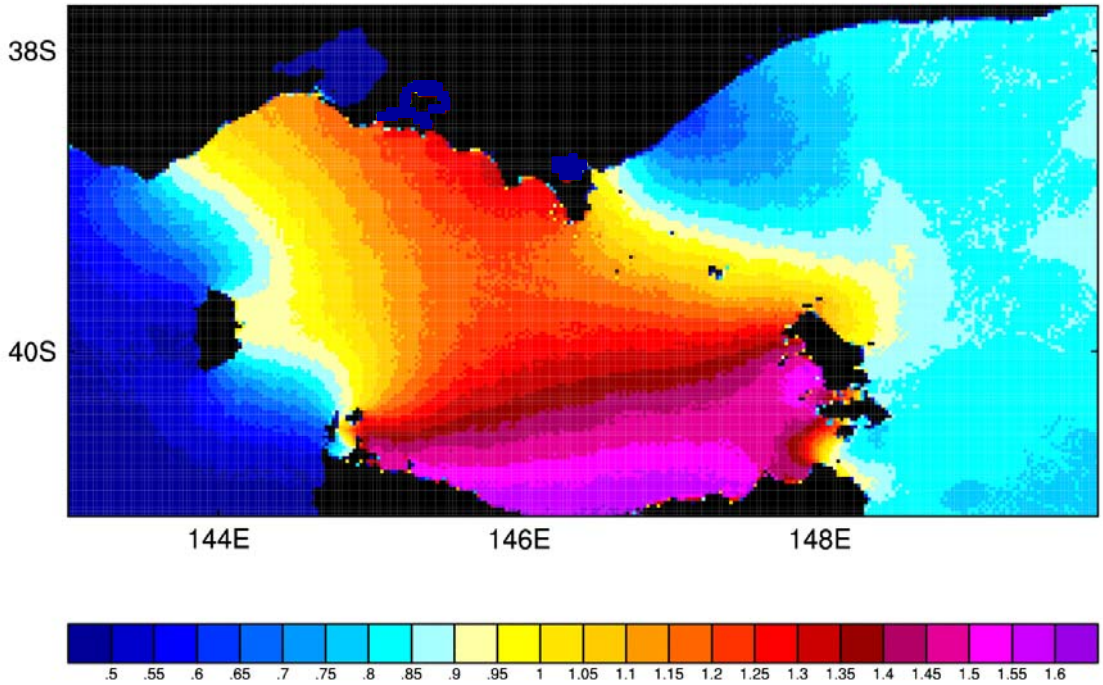

Figure 12: *The spatial pattern for the 99th percentile high tide heights (m). (Note that no values are given for Port Philip Bay, Western Port Bay and Corner Inlet due to inadequate model resolution of these features).*

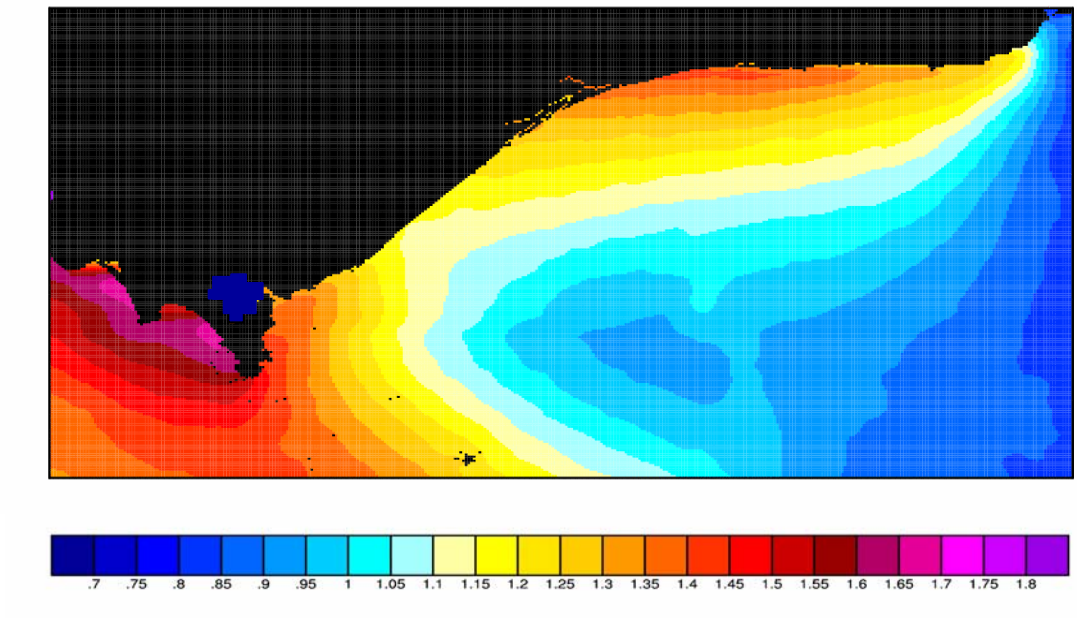

Figure 13: *The spatial pattern of the 1 in 100 year storm tide heights (m) under current climate conditions. (Spatial storm tide probabilities for Corner Inlet are omitted due to inadequate model resolution of this inlet. Tide height probabilities for Port Welshpool were derived from tide gauge data)*

Table 6: *Storm tide height return levels for selected locations along the coast under current climate and 2030 and 2070 scenarios. (Note that tidal probabilities for Stony Point and Port Welshpool were calculated using tide constituents derived from tide gauge data).*

Location	Return Period (yr)	Current Climate (m)	2030				2070			
			Low (m)	Mid (m)	High (m)	High JJA (m)	Low (m)	Mid (m)	High (m)	High JJA (m)
Stony Point	10	1.98	1.96	2.00	2.02	2.02	1.94	2.02	2.09	2.14
	20	2.02	2.00	2.04	2.06	2.07	1.98	2.06	2.13	2.20
	50	2.08	2.06	2.10	2.12	2.13	2.03	2.12	2.20	2.26
	100	2.12	2.10	2.14	2.17	2.17	2.07	2.17	2.25	2.32
Venus Bay	10	1.64	1.63	1.64	1.65	1.66	1.60	1.65	1.73	1.78
	20	1.67	1.66	1.68	1.69	1.70	1.63	1.69	1.77	1.82
	50	1.71	1.70	1.73	1.74	1.75	1.67	1.74	1.83	1.87
	100	1.74	1.73	1.76	1.78	1.79	1.70	1.78	1.87	1.91
Walkerville	10	1.50	1.49	1.51	1.52	1.53	1.47	1.52	1.59	1.64
	20	1.53	1.52	1.54	1.55	1.56	1.49	1.55	1.63	1.67
	50	1.57	1.55	1.59	1.60	1.61	1.53	1.60	1.68	1.72
	100	1.60	1.58	1.62	1.64	1.64	1.55	1.64	1.71	1.76
Tidal River	10	1.62	1.60	1.63	1.64	1.65	1.58	1.64	1.70	1.77
	20	1.65	1.64	1.67	1.68	1.69	1.61	1.68	1.74	1.81
	50	1.70	1.68	1.72	1.73	1.74	1.65	1.73	1.79	1.86
	100	1.73	1.71	1.75	1.77	1.78	1.68	1.77	1.84	1.91
Port Welshpool	10	1.62	1.60	1.63	1.64	1.64	1.58	1.64	1.68	1.74
	20	1.65	1.63	1.66	1.67	1.67	1.61	1.67	1.71	1.78
	50	1.68	1.67	1.70	1.71	1.71	1.64	1.71	1.75	1.82
	100	1.71	1.70	1.73	1.74	1.75	1.67	1.74	1.79	1.86
Lakes Entrance	10	1.30	1.29	1.31	1.32	1.33	1.25	1.32	1.39	1.45
	20	1.33	1.32	1.34	1.35	1.36	1.28	1.35	1.43	1.49
	50	1.37	1.36	1.38	1.40	1.40	1.31	1.40	1.47	1.53
	100	1.40	1.38	1.41	1.43	1.44	1.34	1.43	1.51	1.57

5.4 Mean Sea Level Rise

Mean sea level rise occurs as a result of both thermal expansion of the ocean as it warms and the melting of ice sheets and glaciers. IPCC (2001) estimates of low, mid and high mean sea level rise for 2030 and 2070 are presented in Table 7. These estimates include the uncertainty associated with future emissions of greenhouse gases and uncertainty in the climate response to those changes. Therefore, the assumptions underpinning these changes are consistent with those that underpinned the low, mid and high wind speed scenarios. Comparing these values with the changes in 1 in 100 year storm surge events, it is clear that mean sea level rise will have a larger impact on sea level extremes than wind speed changes. The 2030 mid and 2070 mid storm tide changes are about 12 to 15 % of the respective mean sea level rise scenarios. The 2030 high and 2070 high wind scenarios produce increases in storm tide height that are about 19% of the respective mean sea level rises.

Table 7: *IPCC estimates of low, mid, and high mean sea level rise for 2030 and 2070.*

2030			2070		
Low (m)	Mid (m)	High (m)	Low (m)	Mid (m)	High (m)
0.03	0.10	0.17	0.07	0.25	0.49

The storm tide values from Table 6 have been added to the respective mean sea level rise scenarios and are presented in Table 8 to give a total scenario of extreme sea level change in 2030 and 2070. These yield approximate net changes in the 1 in 100 year storm tide of approximately 1, 12, 21 and 22 cm increase for the low, mid, high and high JJA scenarios respectively for 2030 and 2, 29, 57 to 63 and 64 to 69 cm for 2070. These differences are illustrated in Figure 15 for Venus Bay in 2070, in which randomly sampled storm tide values under each scenario are combined with their respective mean sea level rise scenario. These illustrate that the mid range scenario exhibits only slightly discernable differences from current climate conditions. If wind speed reductions were to occur as with the low range of change, the reductions in storm tide would be almost completely cancelled out by the low scenario for mean sea level rise.

Table 8: *Storm tide return levels for selected locations along the coast under current climate and 2030 and 2070 low, mid and high scenarios including corresponding mean sea level rise scenarios.*

Location	Return Period (yr)	Current Climate (m)	2030				2070			
			Low (m)	Mid (m)	High (m)	High JJA (m)	Low (m)	Mid (m)	High (m)	High JJA (m)
Stony Point	10	1.98	1.99	2.10	2.19	2.19	2.01	2.27	2.58	2.63
	20	2.02	2.03	2.14	2.23	2.24	2.05	2.31	2.62	2.69
	50	2.08	2.09	2.20	2.29	2.30	2.10	2.37	2.69	2.75
	100	2.12	2.13	2.24	2.34	2.34	2.14	2.42	2.74	2.81
Venus Bay	10	1.64	1.66	1.74	1.82	1.83	1.67	1.90	2.22	2.27
	20	1.67	1.69	1.78	1.86	1.87	1.70	1.94	2.26	2.31
	50	1.71	1.73	1.83	1.91	1.92	1.74	1.99	2.32	2.36
	100	1.74	1.76	1.86	1.95	1.96	1.77	2.03	2.36	2.40
Walkerville	10	1.50	1.52	1.61	1.69	1.70	1.54	1.77	2.08	2.13
	20	1.53	1.55	1.64	1.72	1.73	1.56	1.80	2.12	2.16
	50	1.57	1.58	1.69	1.77	1.78	1.60	1.85	2.17	2.21
	100	1.60	1.61	1.72	1.81	1.81	1.62	1.89	2.20	2.25
Tidal River	10	1.62	1.63	1.73	1.81	1.82	1.65	1.89	2.19	2.26
	20	1.65	1.67	1.77	1.85	1.86	1.68	1.93	2.23	2.30
	50	1.70	1.71	1.82	1.90	1.91	1.72	1.98	2.28	2.35
	100	1.73	1.74	1.85	1.94	1.95	1.75	2.02	2.33	2.40
Port Welshpool	10	1.62	1.63	1.73	1.81	1.81	1.65	1.89	2.17	2.23
	20	1.65	1.66	1.76	1.84	1.84	1.68	1.92	2.20	2.27
	50	1.68	1.70	1.80	1.88	1.88	1.71	1.96	2.24	2.31
	100	1.71	1.73	1.83	1.91	1.92	1.74	1.99	2.28	2.35
Lakes Entrance	10	1.30	1.32	1.41	1.49	1.50	1.32	1.57	1.88	1.94
	20	1.33	1.35	1.44	1.52	1.53	1.35	1.60	1.92	1.98
	50	1.37	1.39	1.48	1.57	1.57	1.38	1.65	1.96	2.02
	100	1.40	1.41	1.51	1.60	1.61	1.41	1.68	2.00	2.06

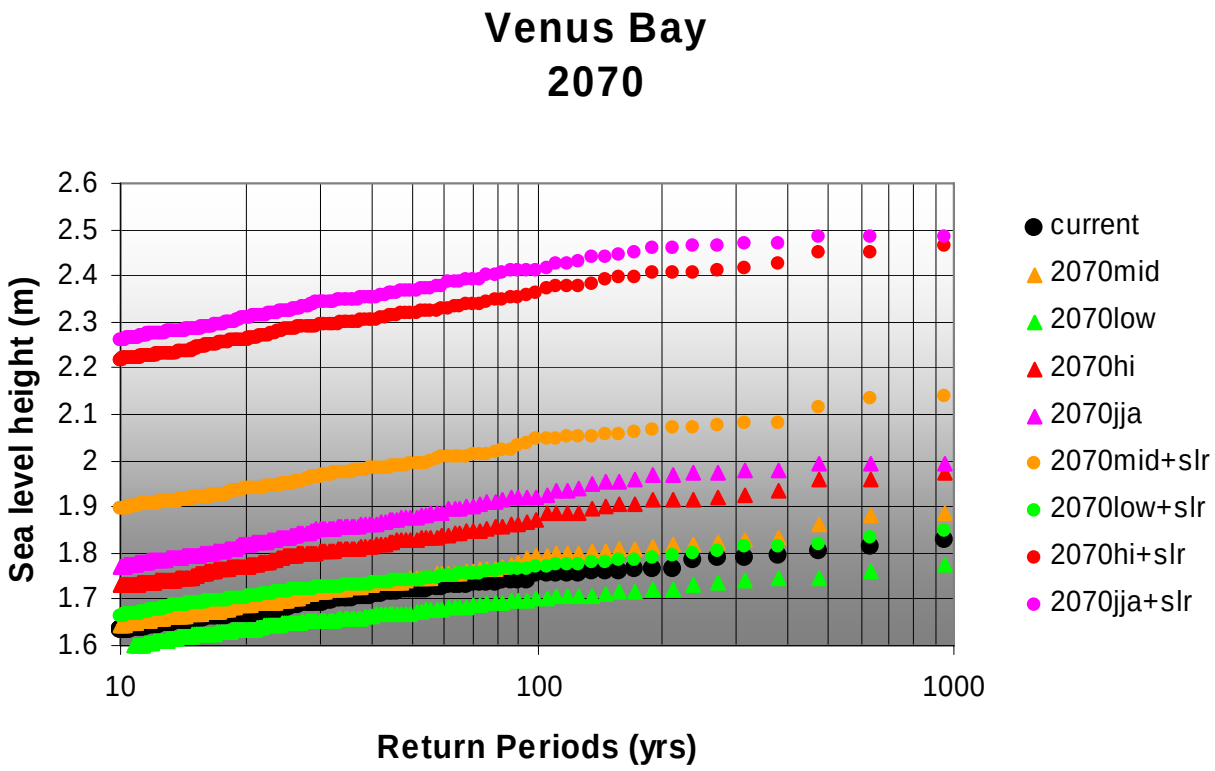

Figure 14: *Randomly sampled storm tide values under the five 2070 scenarios and the net change when mean sea level rise scenarios are incorporated.*

6 Subsidence Potential along the Gippsland Coast

The focus of this study so far has been on the relative changes in sea levels as a result of increases in storm tide heights and mean sea level rise. Also of relevance when considering the risk of coastal flooding is the potential for coastal terrain to subside and thereby further increase this risk. This section provides a summary of recent assessments of subsidence potential along the Gippsland Coast.

Subsidence occurs as a result of the compression of layers of sediment underlying the land surface. It has been observed to accompany the extraction of water and other fluids from subsurface sediments in many parts of the world (Sinclair Knight Merz, 1999b). Although no significant subsidence has been observed by a network of subsidence monitoring sites established along the Gippsland coast in the early 1990s, there are concerns that the coastal land surface will start to subside in the future. These are based on borehole measurements that have shown that groundwater levels in the underlying Latrobe Group aquifer have been in decline since 1975.

The Latrobe Group aquifer is a sequence of sediments composed largely of sand and clay which underlies Gippsland and extends offshore to near the edge of the continental shelf. Offshore the aquifer contains vast amounts of oil and gas while under the Latrobe Valley it contains significant quantities of brown coal. The history of the dewatering of the aquifer associated with the exploitation of these resources is well-documented (Hatton et al, 2004). It began in earnest in 1969 with the commencement of offshore hydrocarbon

extraction and the pumping of water out of coal mines in the Latrobe Valley. Since then the total rate of water extraction associated with these activities and with irrigation and industrial water usage has increased to over 100,000 $MLyr^{-1}$.

Compression of a sediment layer can occur as a result of an increase in the weight of overlying formations or by a reduction in formation pressure, the pressure exerted by fluid within the layer. Monitoring along the Gippsland coast has not indicated that any subsidence has taken place. However, the characteristics of the aquifer underlying this region indicate that it could undergo significant subsidence in the future if the formation pressure continues to decrease as a result of fluid extraction.

Subsidence modelling of two sites along the Gippsland Coast has been undertaken by Sinclair Knight Merz (Sinclair Knight Merz, 2001a and 2001b) to yield future subsidence scenarios (Table 9). However, these results must be interpreted with care since the absence of key geological observations in the region meant that the values of almost all of the relevant geological parameters had to be assumed.

Table 9: *Estimates of subsidence for Golden Beach and Alberton for 2022, 2029 and 2069. The estimates given are mm of subsidence relative to the 1969 level of the land surface*

Site	Estimate	2022	2029	2069
Golden Beach (confined pressure loss assumption)	Low	24	3	3
	Most likely	40	32	4
	High	89	90	90
Golden Beach (extensive pressure loss assumption)	Low	36	3	3
	Most likely	59	47	6
	High	123	127	127
Alberton	Low	98	14	13
	Most likely	289	254	40
	High	835	897	977

Because the compressibility of the Latrobe Group aquifer is spatially variable, different parts of the Gippsland Coast are likely to experience different degrees of subsidence. Ensembles of model simulations based on different sets of assumed values of geological parameters suggest that the land surface at a site in the Alberton area, beneath which the aquifer is thought to be especially compressible, is unlikely to subside by more than about 1 m. However it is possible that the assumed values on which the simulations are based may not reflect the actual geological conditions in the area and that the likelihood of layers of sediment beneath the site entering a highly compressible state might be underrepresented. A relatively simple calculation that assumes that the entire layer of the aquifer experiencing a loss of formation pressure is in such a state suggests that parts of the coastline have the potential to subside by 1 or 2 m (Sinclair Knight Merz, 1995).

7 Conclusions and Recommendations for Further Work

This report has provided a detailed assessment of the impact of wind speed changes on storm surges along the eastern Victorian coastline utilising the most recent assessment of wind speed change for the region. The study showed that the coastline around Lakes Entrance had the highest storm surge potential but when combined with tides, the highest sea levels occurred to the west of Wilsons Promontory. The analysis of storm tide change revealed that under the worst case wind speed scenario, storm tide height would increase by up to 5 cm in 2030 and 20 cm in 2070. The 2030 mid and 2070 mid storm tide changes are about 12 to 15 % of the respective mean sea level rise scenarios. The 2030 high and 2070 high wind scenarios produce increases in storm tide height that are about 19% of the respective mean sea level rises. Hence, mean sea level rise will provide the largest contribution to future flood risk.

Coastal flood risk along the Gippsland coast may be exacerbated in the future by land surface subsidence. Studies have estimated that the coast could subside by between 13 and 977 mm at Alberton by 2070, although there is considerable uncertainty in some of the assumptions that were required to generate these values.

The modelling results in the present study were undertaken at a 1 km resolution, thereby precluding detailed resolution of Corner Inlet and Lakes Entrance. Higher resolution of these two locations would enable the results generated in the present study to be evaluated at locations within these more complex coastal regions.

Several other contributions to coastal flood risk and erosion have not been assessed in this study. These include the impact of wind on waves during severe storm events. Waves can further increase maximum coastal sea levels through the processes of wave set up and wave run up. The occurrence of waves on a higher base sea level will mean that their damaging effects can penetrate further inland causing erosion and damage to infrastructure.

Analysis of the synoptic weather systems responsible for storm surges along the eastern Victorian coast revealed that cold fronts were the dominant cause. However, the less frequent southern Tasman and east coast lows are often the cause of extreme rainfall and therefore may be more likely to produce severe flooding of low-lying areas such as Lakes Entrance due to the combined effects of storm surge and riverine run-off. Extreme rainfall over south-east NSW is projected to increase implying a similar result may be found for east Gippsland. The effect of climate change on the frequency and intensity of the combined events needs to be quantified at higher spatial scale to provide input into coastal risk assessment studies and to inform the development of appropriate coastal management practices in the future.

Finally, further assessment is required of the climate models to understand the tendency for 95th percentile winds to increase more markedly in winter than in the other seasons. Such a change could point to a shift in the seasonality of extreme events making them more frequent at certain times of the year.

Acknowledgments

The work of the authors draws upon research findings of many colleagues within CSIRO Marine and Atmospheric Research and overseas research institutions. CSIRO global and regional climate models were developed by the members of the Climate, Weather and Ocean Prediction Theme of CSIRO Marine and Atmospheric Research.

Tide gauge data have been provided by the National Tidal Centre of the Australian Bureau of Meteorology and by Rodger Grayson and Kim Seong Tan of the University of Melbourne.

The authors would also like to thank Alec Stephenson, for advice on extreme value analysis, Tom Hatton, Claus Otto and Jim Underschultz of CSIRO's Wealth from Oceans Flagship Program, for assistance with the material describing subsidence potential along the Gippsland Coast, and Ben Preston of CSIRO Marine and Atmospheric Research, for reviewing this report.

The Australian Greenhouse Office through the Australian Climate Change Research Program and the Australian Government's Cooperative Research Centres Programme through the Antarctic Climate and Ecosystems Cooperative Research Centre (ACE CRC) contributed funding to this project.

References

Bijl, W., 1997: Impact of a wind climate change on the surge in the southern North Sea. Clim. Res., 8, 45-59.

Coles, S.G., 2001: An Introduction to Statistical Modeling of Extreme Values. Springer.

Godin, G., 1972: The Analysis of Tides. University of Toronto Press.

Grayson, R.B., Candy, R., Tan, K.S., McMaster, M., Chiew, F., Provis, D., and Zhou, S., 2004: Gippsland Lakes Flood Level Modelling Project Final Report. University of Melbourne Centre for Environmental Applied Hydrology Report.

Hatton, T., Otto, C., and Underschultz, J., 2004: Falling water levels in the Latrobe Aquifer, Gippsland Basin: Determination of cause and recommendations for future work. CSIRO Wealth from Oceans Flagship Program Report.

Holmes, J.D., and Moriarty, W.W., 1999: Application of the Generalized Pareto Distribution to wind engineering. Journal of Wind Engineering and Industrial Aerodynamics, 83, 1-10.

Hosking, J.R.M., and Wallis, J.R., 1987: Parameter and quantile estimation for the Generalized Pareto Distribution. Technometrics, 29, 339-349.

Hubbert, G. D., and McInnes, K.L., 1999: A storm surge inundation model for coastal planning and impact studies. J. Coastal Research, 15, 168-185.

Hubbert, G.D., 1993a: Modelling continental shelf flows along the New South Wales coast with a fully three dimensional ocean model. Proc. 11th Australasian Coastal and Ocean Engineering Conference, Townsville, Australia.

Hubbert, G.D., 1993b: Oil spill trajectory modelling with a fully three dimensional ocean model. Proc. 1th Australasian Coastal and Ocean Engineering Conference, Townsville, Australia.

IPCC 2000 [Nakicenovic, N., and Swart, R., (eds)]: Special Report on Emissions Scenarios, Cambridge University Press, Cambridge, 612pp.

IPCC 2001 [Houghton, J.T., Ding, Y., Griggs, D.J., Noguer, M., van der Linden, P.J., Dai, X., Maskell, K., and Johnson, C.A., (eds)]: Climate Change 2001: The Scientific Basis. Contribution of Working Group I to the Third Assessment Report of the Intergovernmental Panel on Climate Change, Cambridge University Press, Cambridge, 944pp.

Le Provost, C., Bennett, A.F., and Cartwright, D.E., 1995: Ocean tides for and from TOPEX/POSEIDON. Science, 267, 639-642.

McInnes, K.L, and Hubbert, G.D., 2001: The impact of eastern Australian cut-off lows on coastal sea levels. Meteorological Applications, 8, 229-243.

McInnes, K.L., and Hubbert, G.D., 2003: A numerical modeling study of storm surges in Bass Strait. Aust. Met. Mag. 52, 143-156.

McInnes, K.L., Abbs, D.J., and Bathols, J.A., 2005: Climate Change in Eastern Victoria Stage 1 Report: The effect of climate change on coastal wind and weather patterns. CSIRO Consultancy Report for the Gippsland Coastal Board.

Sharples, C., 2004: Indicative Mapping of Tasmanian Coastal Vulnerability to Climate Change and Sea Level Rise: Exploratory Report. Report to the Tasmanian Government Department of Primary Industries, Water and Environment.

Sinclair Knight Merz, 1995: Assessment of Subsidence Potential along the Gippsland Coast due to Subsurface Fluid Production. Report to the Victorian Government Department of Natural Resources and the Environment.

Sinclair Knight Merz, 1999: Comparison of Subsidence throughout the World with the Gippsland Basin. Report to the Victorian Government Department of Natural Resources and the Environment.

Sinclair Knight Merz, 2001a: Gippsland Subsidence Modelling – Yarram. Report to the Victorian Government Department of Natural Resources and the Environment.

Sinclair Knight Merz, 2001b: Gippsland Subsidence Modelling – West Golden Beach. Report to the Victorian Government Department of Natural Resources and the Environment.

Tan, K.S., and Grayson, R.B., 2002: Reconstruction of coastal ocean levels offshore of Lakes Entrance for the Gippsland Lakes Flood Modelling Project. University of Melbourne Centre for Environmental Applied Hydrology Report.

Thieler, E.R., Williams, J., and Hammar-Klose, E., 1999: National Assessment of Coastal Vulnerability to Sea-Level Rise. Woods Hole Field Center, US Geological Survey. Available at http://woodshole.er.usgs.gov/project-pages/cvi/.

Whetton, P.H., McInnes, K.L., Jones, R.N., Hennessy, K.J., Suppiah, R., Page, C.M., Bathols, J.A., and Durack, P., In preparation: Climate change projections for Australia for impact assessment and policy application: A review. CSIRO Technical Paper.